

# In-Service Performance Evaluation and Monitoring of a Hybrid Composite Beam Bridge System

[http://www.virginiadot.org/vtrc/main/online\\_reports/pdf/18-r5.pdf](http://www.virginiadot.org/vtrc/main/online_reports/pdf/18-r5.pdf)

---

**DEVIN K. HARRIS, Ph.D.**  
Assistant Professor

**JOHN M. CIVITILLO**  
Graduate Research Assistant

Department of Civil and Environmental Engineering  
University of Virginia

Final Report VTRC 18-R5

**Standard Title Page - Report on Federally Funded Project**

1. Report No.: FHWA/VTRC 18-R5		2. Government Accession No.:		3. Recipient's Catalog No.:	
4. Title and Subtitle: In-Service Performance Evaluation and Monitoring of a Hybrid Composite Beam Bridge System				5. Report Date: October 2017	
				6. Performing Organization Code:	
7. Author(s): Devin K. Harris, Ph.D., and John M. Civitillo				8. Performing Organization Report No.: VTRC 18-R5	
Performing Organization Name and Address: University of Virginia 351 McCormick Road Charlottesville, VA 22904				10. Work Unit No. (TRAVIS):	
				11. Contract or Grant No.: 103944	
12. Sponsoring Agencies' Name and Address: Virginia Department of Transportation      Federal Highway Administration 1401 E. Broad Street                              400 North 8th Street, Room 750 Richmond, VA 23219                                Richmond, VA 23219-4825				13. Type of Report and Period Covered: Final Contract	
				14. Sponsoring Agency Code:	
15. Supplementary Notes:					
<p>16. Abstract:</p> <p>The hybrid composite beam (HCB) technology has been presented as a system for short and medium span beam bridges as an alternative to traditional materials such as concrete and steel. An HCB consists of a concrete tied arch encased in a fiber-reinforced polymer shell. When compared to traditional materials, the HCB system is lighter in weight, which allows for multiple members to be transported on a single truck and smaller cranes to be used during construction, and even reuse of existing substructures. In addition, the protective nature of the FRP outer shell provides additional resistance to corrosion for the reinforcement internal to the system, potentially offering an extended lifespan over conventional girders. Similar to other beam-type bridges for highways, the HCB system is made composite with a conventionally reinforced concrete deck.</p> <p>This study was conducted as a means of evaluating HCB girders for use in a skewed bridge project as a replacement for the existing bridge that crossed Tides Mill Stream along Route 205 in Colonial Beach, Virginia. The existing bridge structure was a short span (~40 ft) simply supported concrete girder bridge with 45° skew and served as a primary connector route for the Colonial Beach community. With respect to the HCB system for bridges, previous testing and applications had been limited to straight bridges, and the Virginia Department of Transportation (VDOT) wished to gather more information on the behavior of these complicated HCBs in a skewed configuration. The primary goal of the investigation was to gain a better understanding of the system behavior including how the loads are transmitted, both at the system and element levels, and also to provide recommendations on how the structure might be inspected and evaluated in the future to ensure the beams are healthy, despite the inability to visually inspect the crucial load carrying components encased in the fiberglass shell.</p> <p>This study was the second phase of the overall study on the HCB system and followed a laboratory study at Virginia Tech, which focused on the behavior of both the individual HCB members and a full-scale girder bridge configuration. The study presented herein focused on an in-service live load test of the bridge constructed by VDOT across Tides Mill Stream. The live load testing program included the evaluation of lateral load distribution, dynamic load allowance, and the internal load sharing behavior of the HCB members. With respect to the live load performance, the HCB system generally conformed to the provisions of the AASHTO specifications for beam-type bridges but did exhibit some characteristics of a flexible system when the dynamic response was considered. It was also noted that the load sharing behavior within the HCB system was non-composite, with the exterior fiber-reinforced polymer shell behaving somewhat independently of the internal tied arch. In addition to the load-testing program, this study provides recommendations on potential non-destructive evaluation methods that may be appropriate for evaluating the condition of this type of structure.</p>					
17 Key Words: hybrid composite beam, HCB, lateral load distribution, dynamic load allowance, load test, non-destructive evaluation			18. Distribution Statement: No restrictions. This document is available to the public through NTIS, Springfield, VA 22161.		
19. Security Classif. (of this report): Unclassified		20. Security Classif. (of this page): Unclassified		21. No. of Pages: 52	22. Price:

**FINAL REPORT**

**IN-SERVICE PERFORMANCE EVALUATION AND MONITORING OF A HYBRID  
COMPOSITE BEAM BRIDGE SYSTEM**

**Devin K. Harris, Ph.D.**  
**Associate Professor**

**John M. Civitillo**  
**Graduate Research Assistant**

**Department of Civil and Environmental Engineering**  
**University of Virginia**

*VTRC Project Manager*

Bernard L. Kassner, Ph.D., P.E., Virginia Transportation Research Council

In Cooperation with the U.S. Department of Transportation  
Federal Highway Administration

Virginia Transportation Research Council  
(A partnership of the Virginia Department of Transportation  
and the University of Virginia since 1948)

Charlottesville, Virginia

October 2017  
VTRC 18-R5

## **DISCLAIMER**

The project that is the subject of this report was done under contract for the Virginia Department of Transportation, Virginia Transportation Research Council. The contents of this report reflect the views of the authors, who are responsible for the facts and the accuracy of the data presented herein. The contents do not necessarily reflect the official views or policies of the Virginia Department of Transportation, the Commonwealth Transportation Board, or the Federal Highway Administration. This report does not constitute a standard, specification, or regulation. Any inclusion of manufacturer names, trade names, or trademarks is for identification purposes only and is not to be considered an endorsement.

Each contract report is peer reviewed and accepted for publication by staff of Virginia Transportation Research Council with expertise in related technical areas. Final editing and proofreading of the report are performed by the contractor.

Copyright 2017 by the Commonwealth of Virginia.  
All rights reserved.

## ABSTRACT

The hybrid composite beam (HCB) technology has been presented as a system for short and medium span beam bridges as an alternative to traditional materials such as concrete and steel. An HCB consists of a concrete tied arch encased in a fiber-reinforced polymer shell. When compared to traditional materials, the HCB system is lighter in weight, which allows for multiple members to be transported on a single truck and smaller cranes to be used during construction, and even reuse of existing substructures. In addition, the protective nature of the FRP outer shell provides additional resistance to corrosion for the reinforcement internal to the system, potentially offering an extended lifespan over conventional girders. Similar to other beam-type bridges for highways, the HCB system is made composite with a conventionally reinforced concrete deck.

This study was conducted as a means of evaluating HCB girders for use in a skewed bridge project as a replacement for the existing bridge that crossed Tides Mill Stream along Route 205 in Colonial Beach, Virginia. The existing bridge structure was a short span (~40 ft) simply supported concrete girder bridge with 45° skew and served as a primary connector route for the Colonial Beach community. With respect to the HCB system for bridges, previous testing and applications had been limited to straight bridges, and the Virginia Department of Transportation (VDOT) wished to gather more information on the behavior of these complicated HCBs in a skewed configuration. The primary goal of the investigation was to gain a better understanding of the system behavior including how the loads are transmitted, both at the system and element levels, and also to provide recommendations on how the structure might be inspected and evaluated in the future to ensure the beams are healthy, despite the inability to visually inspect the crucial load carrying components encased in the fiberglass shell.

This study was the second phase of the overall study on the HCB system and followed a laboratory study at Virginia Tech, which focused on the behavior of both the individual HCB members and a full-scale girder bridge configuration. The study presented herein focused on an in-service live load test of the bridge constructed by VDOT across Tides Mill Stream. The live load testing program included the evaluation of lateral load distribution, dynamic load allowance, and the internal load sharing behavior of the HCB members. With respect to the live load performance, the HCB system generally conformed to the provisions of the AASHTO specifications for beam-type bridges but did exhibit some characteristics of a flexible system when the dynamic response was considered. It was also noted that the load sharing behavior within the HCB system was non-composite, with the exterior fiber-reinforced polymer shell behaving somewhat independently of the internal tied arch. In addition to the load-testing program, this study provides recommendations on potential non-destructive evaluation methods that may be appropriate for evaluating the condition of this type of structure.

## **FINAL REPORT**

# **IN-SERVICE PERFORMANCE EVALUATION AND MONITORING OF A HYBRID COMPOSITE BEAM BRIDGE SYSTEM**

**Devin K. Harris, Ph.D.**  
**Assistant Professor**

**John M. Civitillo**  
**Graduate Research Assistant**

**Department of Civil and Environmental Engineering**  
**University of Virginia**

## **INTRODUCTION**

A relatively new technology in the field of structural engineering, hybrid composite beams (HCB), have been deployed in bridges as an alternative to traditional materials such as concrete and steel. As a brief descriptor, the HCB is essentially a concrete tied arch encased in a fiber-reinforced polymer (FRP) shell. When compared to steel and concrete, the HCB system is lighter in weight, which allows for multiple members to be transported on a single truck and smaller cranes to be used during construction, and even reuse of existing substructures. In addition, the protective nature of the FRP outer shell provides additional resistance to corrosion for the reinforcement internal to the system, potentially offering an extended lifespan over conventional girders. Similar to other beam type bridges for highways, the HCB system is made composite with a conventionally reinforced concrete deck.

This study was conducted as a means of evaluating HCB girders for use in a skewed bridge project in Colonial Beach, Virginia. At the onset of this project, the Virginia Department of Transportation (VDOT) proposed the construction of an HCB bridge system as a replacement for the existing bridge that crossed Tides Mill Stream along Route 205 in Colonial Beach. The existing bridge structure was a 44 ft span simply supported concrete girder bridge with a 45° skew (Figure 1) and served as a primary connector route for the Colonial Beach community. With respect to the HCB system for bridges, previous testing and applications had been limited to straight bridges, and VDOT wished to gather more information on the behavior of these complicated HCBs in a skewed configuration. The primary goal of the investigation was to gain a better understanding of the system behavior including how the loads are transmitted, both at the system and element levels, and to provide recommendations on how the structure might be inspected and evaluated in the future to ensure the beams are in sound condition, despite the inability to inspect visually the crucial load carrying components encased in the fiberglass shell.

This investigation was the second phase of a larger project on the HCB system and followed a laboratory study at Virginia Tech (Ahsan, 2012), which focused on the behavior of both the individual HCB members and a full-scale girder bridge configuration. The study presented herein focused on an in-service live load test of the Tides Mill Stream Bridge



**Figure 1. Original Bridge Crossing Tide Mill Stream Along Route 205**

constructed by VDOT. The study also provided recommendations on potential non-destructive evaluation (NDE) methods that may be appropriate for evaluating the condition state of this type of structure.

### **PURPOSE AND SCOPE**

The purpose of this study was to characterize the in-service structural behavior of the HCB bridge system used on the structure constructed by VDOT on Route 205 over Tides Mill Stream in Colonial Beach. The goal of the investigation was to use traditional live-load testing strategies to validate the design assumptions used in the construction of this bridge and provide corroboration with the results from experimental program at Virginia Tech. The behavior characteristics of particular interest included the flexural lateral load distribution behavior, the element load sharing behavior, and the dynamic load amplification of this skewed HCB application. Also of interest was the relative shear contribution provided by the FRP shell and concrete arch components; however, the data for this last component were not successfully recorded during the load test. In addition to the load-testing program, the preliminary evaluation of potential NDE methods provides a foundation for VDOT inspectors to use in future evaluation of the in-service structure.

### **LITERATURE REVIEW**

The idea of HCB technology made its debut in a bridge construction application as a prototype railroad bridge in 2007 (Hillman, 2008; Otter and Doe, 2009; Otter and Tunna, 2011), making it extremely young for a civil engineering technology. Since the prototype testing at the Transportation Technology Center, Inc. (TTCI) in Pueblo, Colorado, HCBs have been used in another railroad project in Colorado and in highway projects in Illinois, New Jersey, Maine, and Missouri. Many of these HCB applications have not included in-service evaluation or field-

testing of the constructed bridges. Accordingly, with the HCB being a relatively new technology (Hillman, 2003), limited technical literature is available. While HCB is gaining acceptance as a viable design solution and being used in more applications, many projects do not involve accompanying research, or the data are yet to be published.

## HCB Background, Design, and Theoretical Behavior

### Materials and Configuration

As highlighted in the previous section, the HCB system at its core can be described simplistically as a tied concrete arch encased in an FRP shell. A single beam consists of a parabolic concrete arch tied in the tension zone by steel, carbon fiber, or glass fiber prestressing strand. Under bending, the beam distributes loads from the top of the beam through axial compression of the arch down to the supports, where the tension strands restrain the supports. The entire arch system is contained within a glass FRP box shell that protects the main load carrying components and contributes additional shear resistance. Figure 2 provides a visual representation of the orientation of each of the aforementioned components.

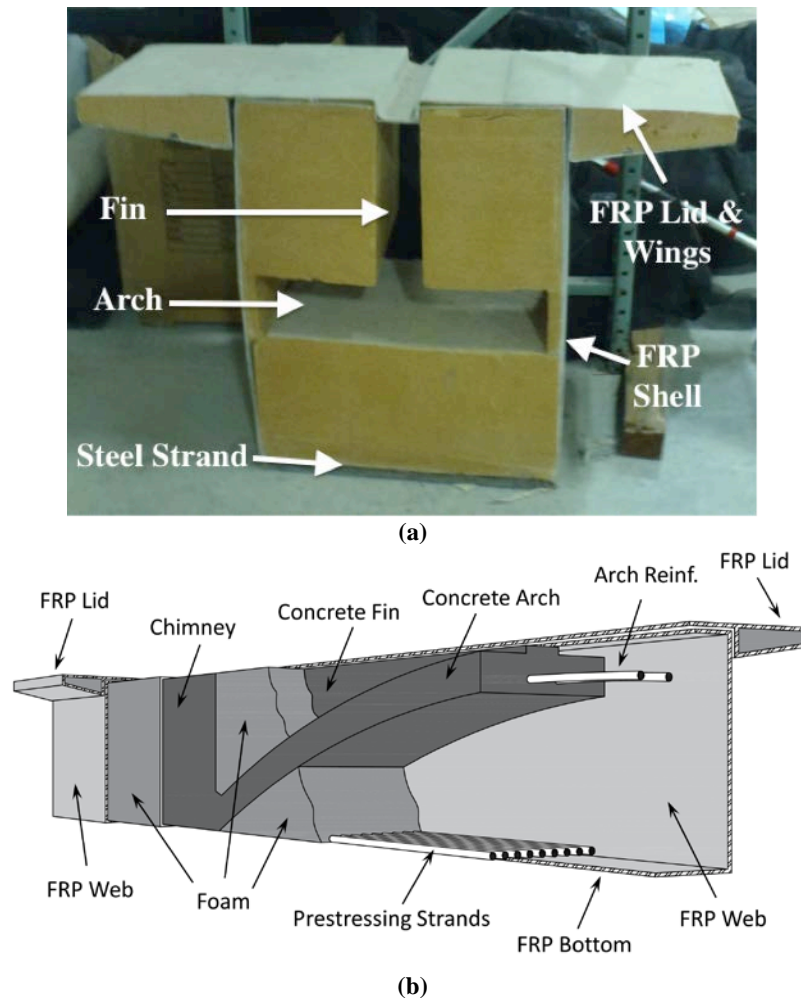


**Figure 2. Hybrid Composite Beam (a) Cross-Section and (b) Isometric System**

For the FRP shell or box, a quad-weave fiber fabric is used to avoid custom alignment of fiber orientations for each application. In this fabric, 45% of the fibers are orientated in the longitudinal direction, while 25% run in both a positive and negative 45-degree orientation from the longitudinal axis. The remaining 30% of the fibers run in the direction perpendicular to the length of the beam (Hillman, 2003). During fabrication of the beam, several layers of the fiberglass fabric are laid in the box formwork. The tension zone reinforcement is laid in the base of the beam formwork and covered with a single additional fiberglass sheet prior to the resin infusion process. Options for the tension reinforcement include carbon fiber, glass fiber prestressing strands, as well as traditional steel strands and a welded steel wire mesh. While each is a valid option, steel remains the most cost effective (Hillman, 2003). The core formwork, cut of polyisocyanurate foam, is laid in the mold next, filling the void space of the box while retaining the arch-shaped formwork for the concrete to be filled in the beam at a later time. The height of the voided concrete formwork varies parabolically over the length of the beam to create the arch shape.

The shell is then infused with a vinyl ester resin through a closed-mold vacuum-assisted resin transfer method, which upon infusion creates a composite unit of FRP, steel, and foam (Hillman and Otter, 2008). During this process, the foam supports the beam shape during the vacuum application, and maintains the arch profile. While the foam alone is not structurally significant, it does offer some lateral stability to the beam, improves the elastic buckling capacity of the FRP webs and helps to distribute the load to the rest of the beam beneath the concrete arch (Hillman, 2003). The companion study by Virginia Tech confirmed this contribution but also noted that the foam is critical for helping the development of the shear resistance through tension field action in the webs.

The FRP lid and wings are manufactured separately from the rest of the beam, but glued together prior to placement of the arch concrete. Inclined shear connectors, consisting of conventional steel rebar, are inserted through holes drilled in the middle of the lid and fed down through the vertical concrete “fin” (Figure 2) to the concrete arch and serve to enforce composite action between the HCB and a conventionally cast reinforced concrete deck. Once the shear connectors are in place, a highly workable concrete mixture, typically self-consolidating concrete (SCC) is fed into the beam to fill the voided conduits. The concrete is vibrated to ensure that all void spaces are filled entirely.

## **Design**

The geometry of these beams is complicated when compared to a conventionally reinforced concrete beam, but the current design methodology includes simplifying design assumptions that allow for use of traditional beam theory (Hillman, 2003). These include assumptions that all materials behave in a linear elastic manner under service loads, and that plane sections remain plane during flexure. A transformed section approach is used, converting steel and concrete sections to equivalent FRP sections. Section properties including centroid and moment of inertia are generated for the tenth points along the beam’s length. Design loading values are drawn from AASHTO, including distribution factors, multiple presence factors, and dynamic load amplifications for an HL-93 design truck, and applied at the tenth points to determine the controlling moment and shears (Hillman, 2011).

The strength limit state for flexure is checked by a comparison of the strains at mid-span to ultimate strain values for each material. The shear strength is limited to the allowable shear stress capacity of the FRP webs, which was defined as 7.5 ksi. Due to the inclined profile of the arch in compression, the vertical component of the axial load is assumed to contribute to the shear resistance, but not the area of the concrete arch or fin. The reason for discounting these two resistance components is to ensure a conservative estimate for the FRP capacity, despite the area of the fin being greatest at the location of maximum shear (Hillman, 2003). It should be noted that these contributions to shear resistance are focal points within the parallel Virginia Tech investigation.

While the proposed strength design approach is intended to ensure safety, a typical HCB system for highway bridges is controlled by a serviceability criterion, specifically deflection. For the HCB system, the stiffness of the beams varies over the length and thus the moment-area method for calculating deflection is used. The deflections are calculated for the non-composite section with no compressive contribution from the deck, and these deflections are used as the camber built into the formwork for the FRP layup. Due to the deflection-controlled design constraint, additional steel is required to satisfy serviceability limits, making the beam over-reinforced from the ultimate strength perspective. Therefore, unlike traditionally designed reinforced concrete beams, the failure mode for the HCB will be a sudden and brittle failure of the deck via crushing before the tension steel ever yields (Hillman, 2003). However, VDOT anticipates that serviceability limit states for deflection and rideability are likely to be reached prior to the strength limit state.

### **Benefits, Drawbacks, and Unknowns**

A topic of interest to some of the preliminary HCB studies (Hillman, 2002) was the feasibility of the system as a viable alternative to existing structural bridge members. There are quite a few features of HCBs that make them attractive to use in both new construction and bridge superstructure replacement projects, but there are also some drawbacks to be considered. Additionally, there are some unknown factors regarding the performance and behavior of the girders that still need to be quantified.

Through use of the concrete arch, a significant quantity of material is saved, which is beneficial from both constructability and environmental standpoints. The minimization of concrete makes the girders much lighter than ordinary prestressed girders typically required for comparable spans. In some cases, there is as much as a 10% to 20% reduction in weight with the deck included (Otter and Doe, 2009). Due to the lighter weight of the girders, shipping costs may be reduced since there will be fewer shipments required. Shipping weight may be drastically reduced if the beams are shipped empty and filled with concrete on site. From an environmental standpoint, the production of cement releases large quantities of carbon dioxide into the atmosphere, so any reduction in concrete consumption is better for the environment. Additionally, the lighter shipping weight and fewer shipments require less fuel consumption.

The low weight of the girders may allow for the reuse of existing abutments in many bridge superstructure replacement projects. Large cranes will not be necessary to move the girders into place, and as the girders are self-supporting both under self-weight and the dead

weight of uncured concrete, the girders may be placed on the abutments without being filled with arch concrete and eliminate the need for any shoring or deck formwork as the girders themselves serve this purpose (Hillman, 2003). Also of importance is the similarity to other bridge construction methods. Once the girders have been fabricated, they resemble a traditional prestressed concrete girder, and require a very low learning curve for installation.

HCBs are also well suited for accelerated bridge construction projects as the girders are self-contained, prefabricated units. If the arch concrete is placed within the girder just off-site with adequate curing time, shipping weight will still be conserved, yet the girders can be installed in a minimal amount of time thus minimizing the disruption to traffic flow (Hillman, 2008).

Of the few negative aspects associated with HCB use, an important one is the previously highlighted over-reinforced nature of the beams. However, while the high reinforcement ratio can lead to a brittle failure, the additional steel increases the ultimate capacity and provides a significant amount of reserve strength. In some cases, that reserve strength can be as much as four times the design strength (Hillman, 2003). The parallel Virginia Tech study is expected to corroborate this characteristic with experimental data. The HCBs tend to be slightly deeper than their prestressed counterparts due to the nature of the arch, which may be of concern to certain users constrained by depth limitations. VDOT provided a rule of thumb for HCB applications that suggests that for the HCB beams should be about the depth of a non-composite steel beam, which is generally shallower than PS bulb tees beams, and deeper than voided slabs or PS box beams in a side-by-side configuration.

Another drawback is the higher cost of HCBs due to the materials and the labor involved in manufacturing the FRP shell, which have to be laid up by hand and the shell manufacturing process has yet to be automated (Hillman, 2003). That being said, should the shell manufacturing process become automated, and as the beams gain traction and are used in an increasing number of projects, the economy of scale should allow for more streamlined manufacturing processes and reduced costs. Still, cost analyses show that the beams are feasible for railway applications in the range of 40 to 60 ft spans, where concrete beams are too heavy for existing rail cranes and steel construction steel is too costly (Otter and Tunna, 2011). Additionally, when taking into account the lifecycle cost of the beams, it has been shown that HCBs are cost-competitive in the 30 to 50 ft span range because the higher cost may be distributed over a longer projected service life (Hillman, 2003), which is expected to approach 100 years versus the projected 75-year lifespan of concrete girders designed according to the AASHTO LRFD Bridge Design Specifications.

The 100-year lifespan projection has yet to be validated, but it has been derived from the FRP shell's ability to protect the internal load carrying components of the beam. The fiberglass is impervious to water and chlorides, thus there is little chance for corrosion of the steel or degrading concrete reactions. In addition, galvanized prestressing steel was used for this particular project to provide additional resistance to corrosion. Furthermore, the FRP weathers well in marine environments, and although is susceptible to degradation from ultraviolet rays, should be adequately protected from sunlight with the concrete bridge deck on top. However,

other questions have been raised, including fire resistance and lateral stability in the case of a vehicular collision (Otter and Doe, 2009).

## **Previous Applications and Investigations**

### **IDEA Program – Preliminary Studies**

The first investigation of hybrid composite girders was sponsored by the Transportation Research Board as part of the Innovations Deserving Exploratory Analysis (IDEA) program. The program involved several phases of investigation and was intended to serve first as a feasibility study for HCB application in the bridge market, and second to test prototype beams to determine the reliability of the design philosophy and gather information on the behavior of the complicated beam systems.

The first phase of this IDEA program was a feasibility study that evaluated the cost of producing beams for varying span lengths. Current railway bridge replacement projects became the focus and led to short and medium span bridge applications. The girders were found to be less costly than steel, but costlier than concrete. Hillman (2003) indicated the life cycle costs could still be competitive. In the second phase of the program, a single 20 ft prototype beam was constructed in 2003 for testing at the University of Delaware. The girder was 12 in wide by 24 in deep and did not include a composite deck. The beam was simply supported, and loaded in nine different configurations using four actuators distributing load over the span with spreaders. Extensive instrumentation included linear strain gauges throughout the interior of the beam to measure bending stresses and maximum stresses in each material, and deflections were recorded with string potentiometers. The test configurations included varying loads across the span, mimicking dead loads of a completed rail structure, live loads produced by a Cooper E-80 rail car with impact factors applied, as well as locations of maximum shear and moment. A cyclical load was applied for 100,000 cycles and then the beam was tested for fatigue damage. On the final loading, the beam was tested to failure, sustaining almost 60 kips of load and measuring a deflection just over 2 in. Although the deflections were greater than predicted, the load tests confirmed the overall design methodology, with the linearly elastic assumptions holding true until just near ultimate loading. An interesting outcome of the study was the discovery that the system acts like a tied arch close to mid-span, but not close to the supports, where the concrete and steel loads diminished as the FRP webs distributed the loads to the supports through shear (Hillman, 2003).

A follow-up study supported by the High-Speed Rail IDEA program was conducted at the Transportation Technology Center, Inc. (TTCI) in Pueblo, Colorado (Hillman, 2008). In this investigation, a complete HCB bridge system was used as a replacement bridge for an existing structure operating on the TTCI test track. The bridge, which weighed just 57% of the one it replaced, consisted of 8 HCBs, each 20 in wide by 28 in deep, and bolted side-by-side through their webs into two four-girder groupings. A 4 in composite deck was included, along with ballast curbs and ballast for the rail. The bridge was located on a curved portion of track and thus experienced a slightly inclined loading from the inclined rail and lateral loading from the train as it traversed the curve. Instrumentation for this test included strain gauges and deflection

sensors located at strategic positions. The loading program consisted of running heavily loaded freight cars over the bridge, first at static locations to produce maximum shear and moment, then at increasingly rapid dynamic speeds. The testing program demonstrated that the structure behaved in a predictable manner and conformed to the AREMA recommended guidelines. The deformation measurements confirmed that there was indeed full composite action between the deck and girders and all of the strains (stresses) measured were well within the ultimate capacities of each respective material. Limited damage was discovered in the deck concrete, but this shear cracking was due to the eccentricity of the load and not due to any HCB deficiencies. The exterior girders, which supported the ballast curbs, always experienced less deflection and strain due to the added stiffness contributed by the curbs.

### **Advanced Structures and Composites Center – Laboratory Study**

A large-scale project was undertaken in 2010 in Boothbay, Maine, to construct an eight-span HCB bridge spanning a total of 540 ft (Snape and Lindyberg, 2009). As part of this project, a single beam was tested by the Advanced Structures and Composites Center at the University of Maine. The experimental program included testing for service and fatigue loads both with and without the addition of a composite deck, and finally an ultimate capacity load test. For this project, the girders were 33 in deep with 42 steel strands of 1/2 in diameter, spaced at 4 ft center-to-center such that the FRP wings were integrated with the lid to serve as formwork for the deck in the interstitial space of the beams. Instrumentation included strain gauges internally and externally, LVDTs, string potentiometers, load cells and a 3D digital imaging system to capture surface strains. Instrumentation was primarily concentrated at mid-span, quarter-spans and the supports. The beam was first tested without the presence of a deck, and was subjected to four-point bending to simulate an HL-93 truck loading. First service shear and moments were determined from static loading, followed by a fatigue loading of 2,000,000 cycles with interim flexural tests to investigate any damage accumulated. The deck was then added to the beam and a similar loading scheme was prescribed. In both cases, the beam achieved the predicted strength, although the beam was stiffer than predicted. The higher stiffness was attributed to the contribution of the FRP wings that were neglected in design calculations (Snape and Lindyberg, 2009). In addition, there was elastic buckling observed in the FRP lid of the beam during the test prior to addition of the deck, but further buckling was constrained by the deck. The last loading cycle took the beam to ultimate and proved that the beam behaved linearly elastic through failure.

### **Virginia Tech – Laboratory Study**

As part of the parallel study on the HCB system for VDOT, an initial experimental investigation was performed by Ahsan (2012) at Virginia Tech, who was tasked with investigating the HCB system in a laboratory setting, focusing on the element-level behavior and load path generated between the concrete arch and FRP shell, at various phases throughout the construction of the system and a variety of loading scenarios. Of particular interest was a confirmation of the flexural design methodology, which currently uses a transformed sections approach (Van Nosedall et al., 2013). Three HCBs were built for testing according to the specifications used for the proposed construction of the Tides Mill Stream Bridge. An extensive research plan was devised to test the beams throughout the fabrication, and ultimately test a

three-girder, fully composite bridge superstructure that would mimic that of the eight-girder bridge design to cross Tides Mill Stream. The work done on these girders can be separated into three distinct phases. First, the empty FRP box shell (including tension steel) was tested. After placement and curing of the SCC within the arch formwork, a second round of tests were performed to investigate the behavior of the tied arch subjected to construction loads. Last, a skewed, three-girder, fully composite bridge superstructure that mimicked the eight-girder design of the Rt. 205 bridge configuration was tested, including a composite deck (Ahsan, 2012). Each of these tests was conducted within the elastic range for the structure and components. An extensive instrumentation plan was devised to test the beams at each phase. Strain gauges were mounted externally on the FRP at multiple locations on the webs, top and bottom flanges, and internally on the tension steel. Vibrating wire gauges (VWGs) were also embedded in the arch concrete. Photogrammetry was employed to allow for complex measures of deflection and subsequent derivations of strain on the face of the FRP web. These measurements were confirmed by traditional deflection measurements, including string potentiometers and linear variable differential transformers (LVDTs). Load cells were also used at the bearings to provide a measure of the shear through the beams at the supports.

For testing of the empty FRP box, the lid and wings were placed on top of the shell, but not glued down, all of the dead load could be accounted for, but not add to the flexural rigidity of the box. These beams were tested in a non-skewed configuration, with the same clear span as the Rt. 205 Bridge. The loading consisted of steel angles spaced closely along the length of the beam. Ahsan found that the FRP behaved in a linear elastic manner under this loading configuration.

The next phase tested a series of completed HCBs, which included the arch concrete and the FRP lids glued to the top of the beams. These beams were also tested in a straight configuration with the same clear span. The two loading scenarios for these beams involved a single load point of 15 kips at mid-span, and two third-point loads of 12.5 kips. As anticipated, the FRP did not contribute significantly to the flexural strength of the overall beam, with the tied concrete arch carrying approximately 80% of the total flexural load, leaving the shell to carry the remaining 20%. In comparing the strain registered on the steel itself and the FRP surrounding the steel, there is relatively good strain compatibility in the tension zone (Van Nossdall et al., 2013).

The final experiments consisted of tests of a three-girder mockup of the fully composite HCB system as would be put in-service at Colonial Beach. It is important to note, however, that the bridge mockup did not include any parapet walls nor was there any mechanism to enforce the fixity caused by the integral abutment backwalls that were part of the actual bridge design. The AASHTO HL-93 design truck was used as the loading configuration with an additional 33% increase to account for dynamic amplification effects. Several simulated wheel path configurations were tested to induce a variety of moment and shear distributions throughout the system. Once the beams became composite with the deck, the neutral axis moved up within the deck. Thus, the HCB ceased to act as a tied arch, and the concrete arch contributed little to the strength of the system. The researchers also found that the FRP shell and tension steel combined to provide 80% of the total flexural resistance, while the deck accounted for the remaining 20% (Van Nossdall et al., 2013). A number of additional findings were also reported by (Ahsan, 2012)

that have direct relevance to the field testing in this current study, described in later sections of this report.

It was determined that the concrete arch does not act compositely with the rest of the HCB system. Ahsan (2012) hypothesized the existence of a local bending phenomenon of this thin arch that is accentuated at the unsupported quarter-spans. The tension strains registered in the bottom of the arch are not compatible, but quite exaggerated compared to the strains read from the external FRP strain gauges, indicating the existence of this phenomenon. Further, there exists a discrepancy between the upper and lower strain readings in the arch also indicating flexure within the arch. Figure 3 shows an adaptation of the phenomenon described by Ahsan.

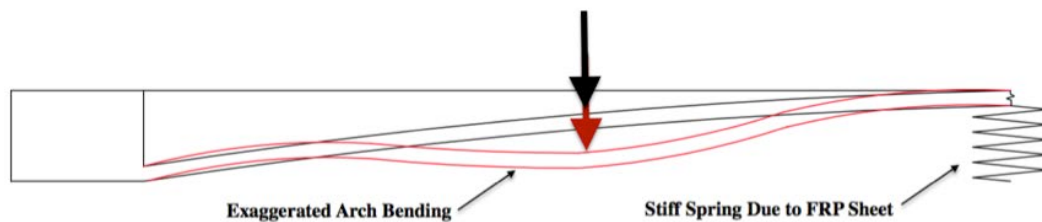


**Figure 3. Thin Arch Local Bending Hypothesis (Adapted from Ahsan, 2012)**

In this theory, the mid-span of the arch is treated as being supported by a stiff spring, as an 8 ft FRP sheet connects the two FRP webs directly beneath the arch conduit. From a practical perspective, the purpose of this sheet was to provide a rigid surface to protect the foam formwork from the force of the concrete placed at this location, and preserve the shape of the arch. Following this theory, it is easy to see how flexure could be induced throughout the length of the arch, but especially at the unsupported quarter points. Some of the theories proposed by Ahsan (2012) include:

1. The tensile strains registered in the bottom of the arch were found to be well above that necessary to induce cracking in this concrete, yet there clearly was a means to carry this level of strain during the test. The strain readings indicate that the two steel strands laid out in the bottom of the arch profile for construction purposes may also provide tensile resistance within the arch (Ahsan, 2012).
2. Ahsan (2012) included an analysis of moment and shear distribution factors from limited load configurations performed on the three-girder system and provided a comparison to the assumed AASHTO values. While the design for this bridge was conservative and did not include skew corrections, Ahsan included lever rule corrections in his calculations and found the exterior girder shear and moment distribution factors to be within AASHTO regulations. Interior distribution factors were less conservative as compared to the AASHTO values.

## **METHODS**

### **Fabrication and Construction of the Tides Mill Stream–Route 205 Bridge**

The live load testing program focused on the newly constructed HCB bridge on Route 205 over Tides Mill Stream in Colonial Beach (Figure 4). Beam fabrication took place in a series

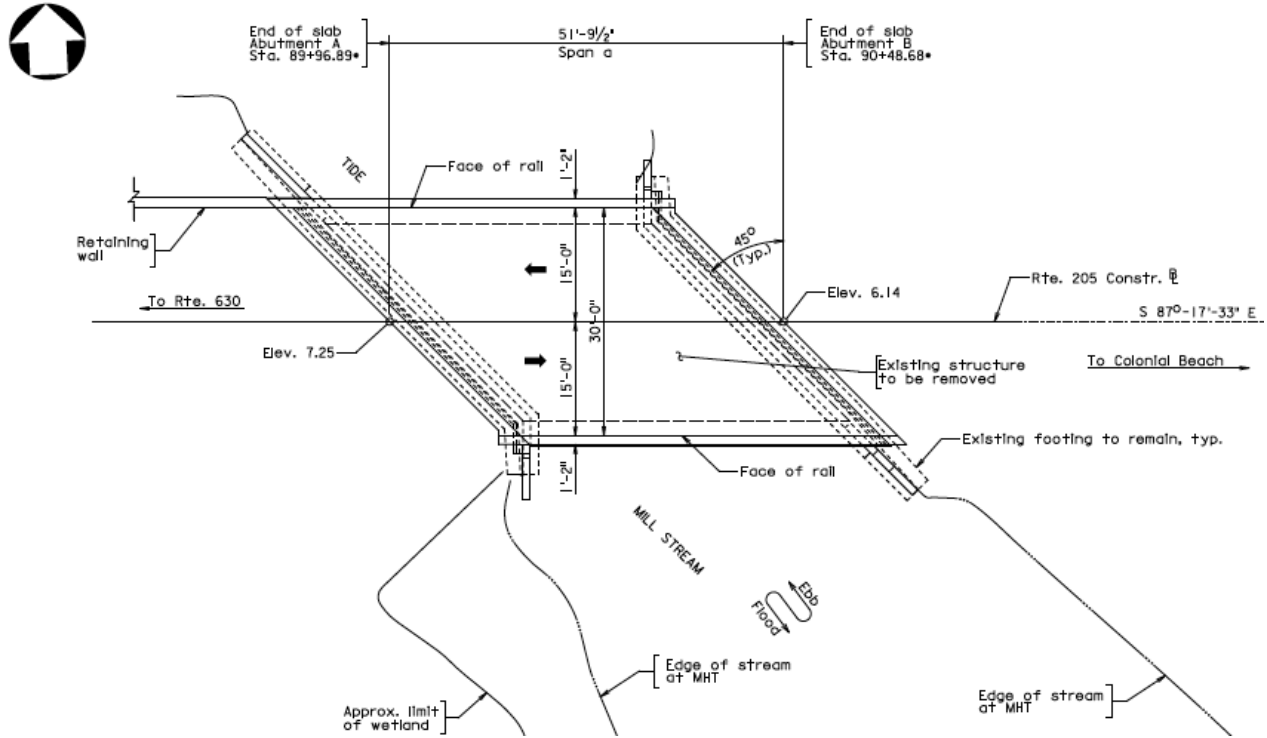


**Figure 4. Tides Mill Stream Site – Plan View**



**(a)**



**(b)**



**(c)**



**(d)**

**Figure 5. HCB Fabrication Process: (a) Glass Fiber Fabric, (b) Foam Inserts, (c) Completed HCB Box, and (d) Placement of SCC Within HCB Arch**

of stages (Figure 5), so the internal instrumentation followed this construction sequence. The HCBs shells and lids were fabricated off site, at Harbor Technologies in Brunswick, Maine. During this fabrication phase, the box shells were laid up with fiberglass and high-strength passive steel strand and foam were placed in the formwork and then infused with resin. In this manner, eight lightweight, self-supporting, monolithic box shells were created and shipped to Coastal Precast concrete plant in Virginia, where they were filled with SCC and allowed to cure, forming a fully functional, composite HCB girder. These girders were placed on the existing abutments that were being reused and the ends were encased in integral backwalls, resulting in semi-integral abutments. From that point, the steel reinforcement mat for the deck was constructed, and construction began to take the form of a conventional bridge project.

The previous concrete girders and deck were replaced with eight HCBs spanning 44 ft over a small creek and supporting a 7.5 in deep conventionally reinforced, cast-in-place concrete deck, while maintaining the existing substructure. Each HCB girder was 21 in deep by 24 in wide and contained inclined shear connectors that enforced composite action between the HCB and the concrete deck. The girders were spaced at approximately 4 ft center-to-center, yielding a 32 ft 4 in transverse width that allowed for two lanes of traffic with 3 ft shoulders (Figure 6). The girders were skewed at 45° and supported by two parallel abutments, and the ends were encased in integral abutment backwalls, resulting in semi-integral abutments. The girders crossed the waterway with a very low clearance of approximately 6 ft at low tide, making access for instrumentation a challenge. The stream feeds to the Potomac River, which flows to the North of the bridge site.

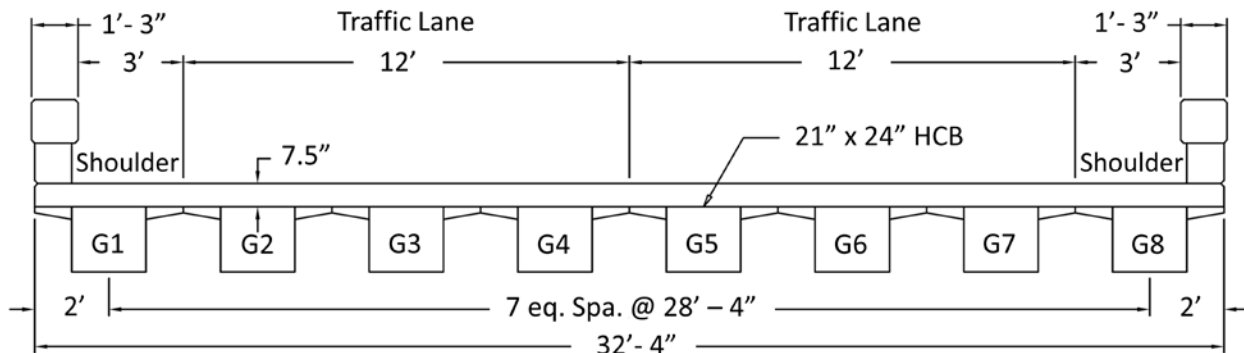
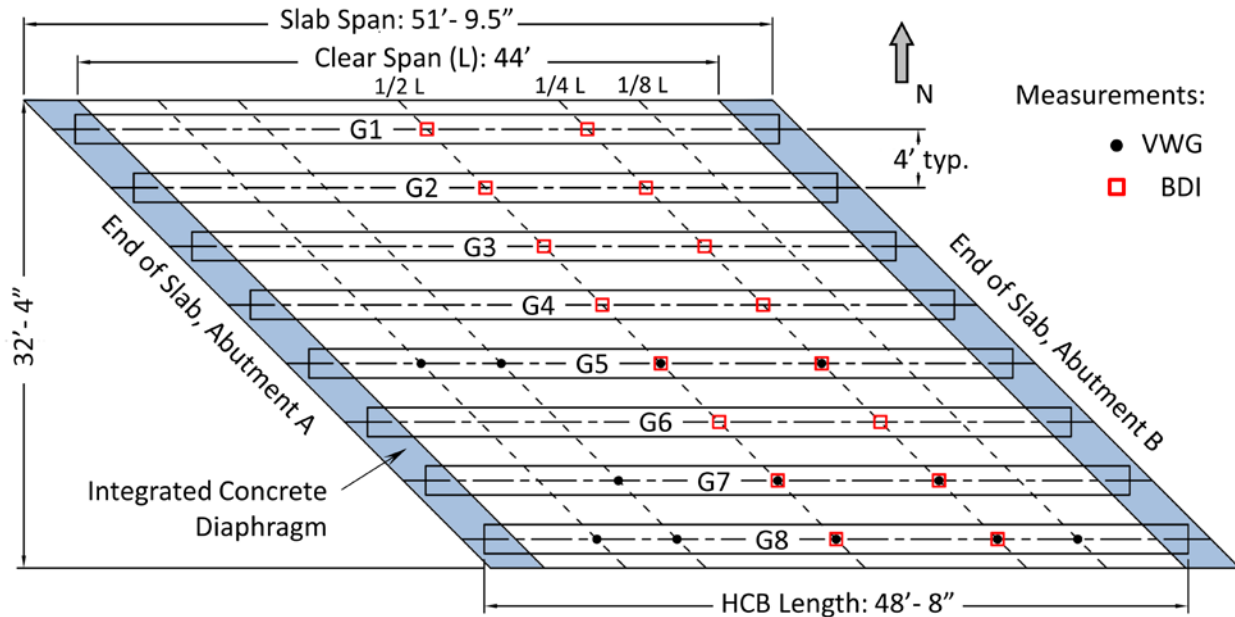


Figure 6. Tides Mill Stream – HCB Bridge Cross-Section

### Instrumentation and Experimental Setup

The focus of this investigation was the initial in-service performance assessment of this particular HCB bridge; however, the instrumentation program that was implemented was chosen to serve two purposes: (1) to yield measured responses during load testing, and (2) to provide long-term monitoring capabilities for the HCB bridge system. To keep the instrumentation systems organized, a nomenclature for the girders was established (Figure 7) where the northernmost girder was labelled number 1 (alternatively girder A per VDOT Plans), and the numbers progressed sequentially to the eighth and southernmost girder, labelled girder 8 (alternatively girder H per VDOT Plans).



**Figure 7. Bridge Nomenclature With Instrumentation Overview (Plan View)**

To satisfy the testing program and establish a mechanism for monitoring, an extensive instrumentation plan was developed. The program required a variety of sensors with multiple data acquisition systems. The various acquisition systems and their functionality are described in further detail in this section. The first data acquisition system used a series of Campbell Scientific Inc. (CSI) dataloggers that monitored internally mounted VWGs that were installed throughout the fabrication and construction phases of the girders and bridge deck. The second data acquisition system was deployed on the day of testing only and used a rapidly deployable wireless field-testing setup by Bridge Diagnostics Inc. (BDI), which primarily used externally mounted strain gauges. It should be noted that both the internal and external gauges were intended to be used during load testing but only internal VWGs were intended for long-term monitoring due to their durability and the protection offered by embedment.

### **Campbell Scientific Data Acquisition and Gauge Installation**

The CSI system provided the capability to measure internal system response during both short-term live load testing and long-term monitoring. Geokon 4200 series embeddable VWGs were used and two separate Campbell Scientific Inc. (CSI) data acquisition systems (DAQ) were selected for measurement. The first CSI DAQ (CR 1000/AWV200/AM32B) was intended for long-term periodic monitoring and provided static-only measurements of select VWGs. This system was limited to a total of 48 VWGs. Similarly, the second CSI DAQ (CR 3000/SC-CPI/CDM-VW305) provided the ability to interrogate VWGs statically, but also provided the capability of interrogating the VWGs dynamically. This dynamic capability was a new capability available from CSI and this investigation provide a preliminary trial of the system. While these systems proved functional, the acquisition of data during the live load testing program was unsuccessful due to programming errors resulting in the data being overwritten. Nonetheless, this information is included herein because the sensors are available for long-term monitoring and future load testing.

The locations of VWGs were selected in collaboration with the study’s technical review panel to capture enough of the desired behavior, while remaining reasonably economical. A total of 48 VWG locations were selected and these VWGs were installed in three of the eight girders (girders 5, 7, and 8) so as to minimize the interference with the construction of the girders. Symmetry of the bridge made this instrumentation plan feasible, as it was still possible to capture both acute and obtuse corners of the skew. Figure 8 and Table 1 illustrate and describe the location of the gauges within the HCB cross-section, while Figure 7 illustrates the selected longitudinal and transverse locations.

Along the length of the three selected beams, gauges were installed at mid-span to yield the maximum flexural responses of these select girders, and at both the quarter-span locations to capture the effect of the skew. Additional gauges were installed at select eighth-span points in a 60° rosette configuration on these three girders to measure shear response.

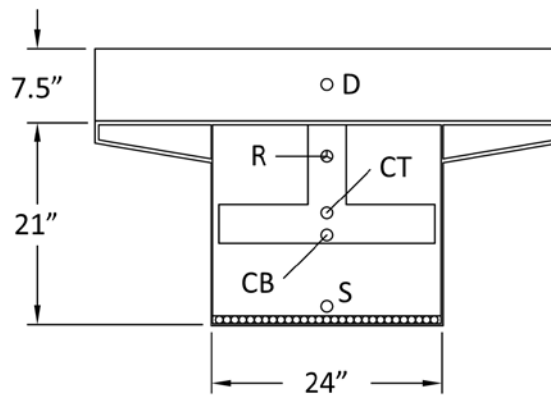


**Figure 8. General Vibrating Wire Gauge Locations Through the Depth**

**Table 1. Vibrating Wire Gauge Instrumentation Location Matrix**

<b>Longitudinal Location</b>	<b>Girder 5</b>	<b>Girder 7</b>	<b>Girder 8</b>
East Eighth-span	-	-	R, CT, CB
East Quarter-span	D, CT, CB, S	D, CT, CB, S	D, CT, CB, S
Mid-span	D, CT, CB, S	D, CT, CB, S	D, CT, CB, S
West Quarter-span	D, CT, CB, S	D, CT, CB, S	D, CT, CB, S
West Eighth-span	R, CT, CB		R, CT, CB

D = deck; CT = upper arch; CB = lower arch; S = tension strand; R = rosette within the fin.

During the first phase of fabrication of the HCBs, the fabrication of the FRP box shell, a VWG was installed at each of the nine proposed mid-span and quarter-span locations at the level of the steel strand. This involved tying the VWG parallel to a tension steel strand as close to the middle of the girder as possible during the layup of the fiberglass sheets and high-strength steel strand (Figure 9). Just as concrete transfers strain to a VWG through the movement of concrete perpendicular to the end discs, it was theorized that when cured, the resin would offer the same transfer of strain to the gauge and an accurate reading would be provided for the particular cross-sectional depth.



**Figure 9. Internal VWG Placement at Tension Level**

After infusion of the FRP shell, the remainder of the VWGs internal to the HCB itself were installed. A series of non-corroding, acrylonitrile butadiene styrene, 3D-printed frames were designed to hold the VWGs in place at the desired location within the voided conduits that would later be filled with SCC. Again, nine frames were placed at the proposed mid-span and quarter-span locations with two VWGs stacked 2 in apart. Each frame was then inserted through the void for the concrete fin (Figure 10a) down to the level of the arch void and inserted into the existing foam formwork such that the VWGs were aligned longitudinally and horizontally with the beam, not parallel to the slope of the arch. Note that the exact cross-sectional depth of these gauges differed by location due to the varying profile of the parabolic arch. At the three designated eighth point locations, a frame identical to the one devised for the other arch locations was used in conjunction with an additional frame on top of the first. This added frame held three VWGs arranged in a 60° rosette. The rosette was designed to measure the shear in the fin near the point of maximum shear and where the fin is deepest. The two frames were linked by two stainless steel threaded rods that enabled the whole assembly to be lowered into the deeper eighth-span locations (Figure 10b).

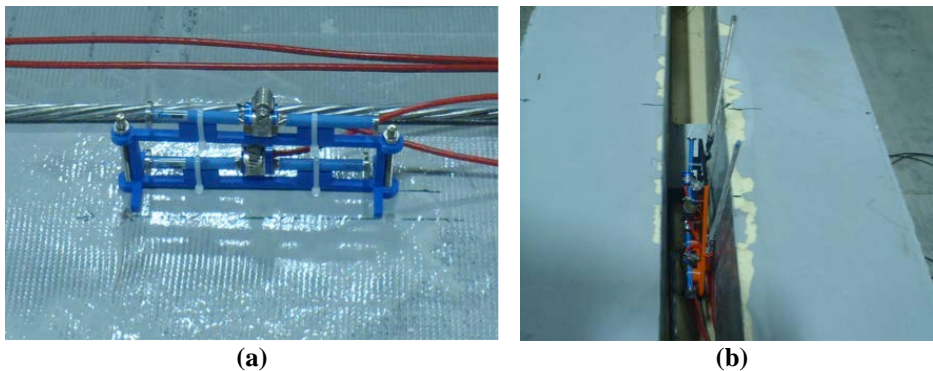


**Figure 10, Stacked Strain Gauge Configuration: (a) Concrete Arch VWG Frame at Mid-span and (b) Additional Rosette Configuration at Eighth-span**

After placement of the internal concrete within the HCB, the beams were positioned on site, and the deck reinforcement mat was laid out. Nine additional gauges were longitudinally affixed to the mat 4 in deep at companion locations to the mid-span and quarter-span locations of the three selected girders prior to placement of the deck concrete (Figure 11). The resulting system of gauges was expected to provide a more comprehensive measure of the overall internal system behavior including the neutral axis location and level of composite action between the deck and girders. However, despite the successful implementation of the internal VWGs, data for only 15 sensors were recorded during the test due to limitations associated with the CSI acquisition system, which was limited to 16 input channels. In addition, no data were collected from the Rosette-configured strain gauges.

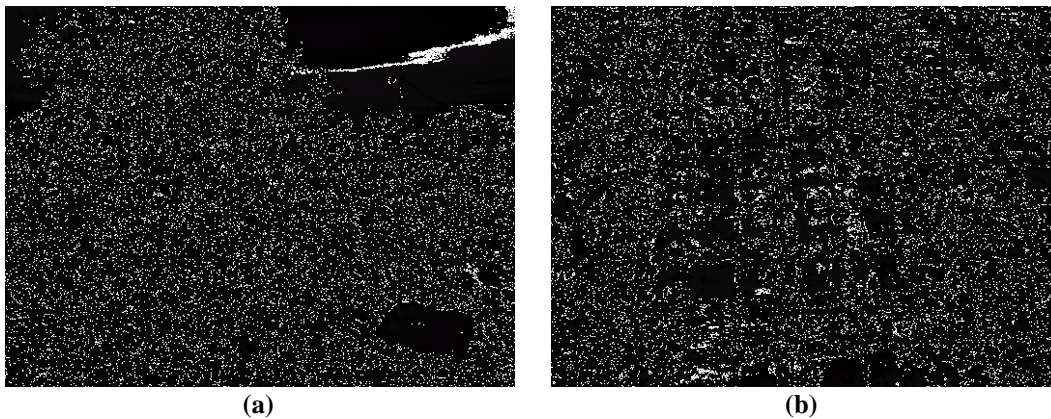


**Figure 11. Instrumentation for Concrete Bridge Deck: (a) Gauge Layout and (b) Installed VWG**

### **Bridge Diagnostics Data Acquisition System and Gauge Installation**

The second data acquisition system was deployed on the day of testing only and used a rapidly deployable wireless field-testing setup by Bridge Diagnostics Inc. (BDI), which primarily used externally mounted strain gauges. The external BDI strain gauges were placed in conjunction with the internal VWGs in order to mirror the strain locations and provide a comparison between the internal strains and the strains experienced by the external FRP shell (Figure 7 and Figure 12). These external gauges were mounted on the bottom flange of each girder at mid-span and the East quarter-span to capture distribution behavior laterally across the eight girders. Additional gauges were mounted on the web of the girders at these locations as close to the arch position as possible, though the depth of the wings made this somewhat challenging at mid-span. These web gauges were used to create an external strain profile that could be aligned with the internal strain profiles and contribute to the evaluation of the load sharing behavior of the individual HCB elements. Last, two additional external BDI strain gauges were placed on the parapet at mid-span such that any strains registered could give an indication of the level of stiffening provided by the barriers to the bridge system. A BDI string potentiometer was also used to measure deflection for the northern exterior girder; however, the anchorage system for the string pot was insufficient to maintain the required tension and was therefore not included in this report.

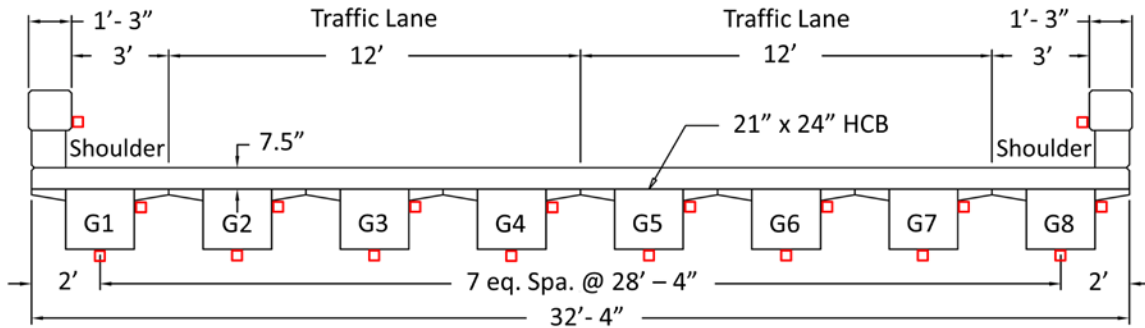


**Figure 12. Tides Mill Stream Bridge Cross-Section With Midspan External Strain Gauge Configuration**

### Experimental Set-up

The instrumentation was performed over two days, August 5 and 6, 2013. The first day consisted mostly of setup and preparatory work and the second day included final preparation and carrying out the load test runs. It was a function of the bridge site that the clearance of the waterway was already shallow, but the clearance between the bridge and stream also fluctuated with the rising tides. This was a concern that had to be factored into the schedule of the load test, and dictated when certain tasks could be performed underneath. This factor determined the need to carry out the load test over two days. The depth of the waterway varied, and as such, a combination of small jon boats and researchers in waders was used for access to attach the sensors beneath the bridge (Figure 13).



**Figure 13. Instrumenting Bridge Underside**

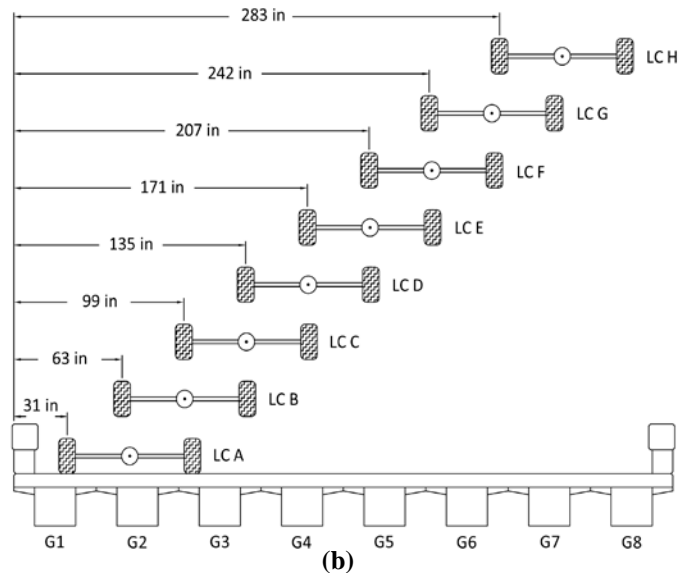
On the morning of August 5, two teams worked to accomplish multiple tasks. One team was responsible for affixing the BDI strain gauges to the underside of the bridge using a very rapid-set epoxy. The bottom flange gauges were aligned and centered on the flange (Figure 14), while the additional longitudinal gauges were adhered 1.5 in beneath the wing edge on the south-facing web. The underside installation and began marking mid and quarter-span locations with measurements taken from the clear span distance, and a chalk line was dropped across all eight

girders, along the skew to mark these locations on each beam. To keep the sensor lead wires organized and dry, conduit clamps were glued along the girders and the lead wires were sequentially zip-tied to the clamps, channeling the groupings out the South end of the bridge where they were bundled and bagged to keep moisture out overnight. These bundles were then hung on conduit clamps on the first interior web, or rested on the abutment face to remain out of sight.



**Figure 14. Bottom Flange External Strain Gauge Placement**

The second team was responsible for marking the pre-determined wheel paths or load cases (Figure 15) and organizing the BDI wireless nodes as input channels (Figure 16). It was important to place specifically labeled gauges at the predetermined locations for data analysis; however, the BDI system does not require one to plug in the gauges in any particular order.



(a)

(b)

**Figure 15. Wheel Path (a) Markings and (b) Configuration**

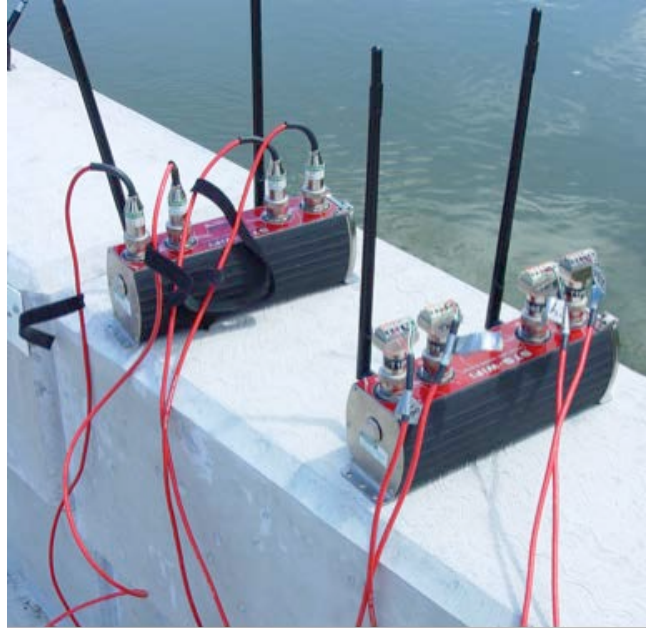


**Figure 16. Wireless BDI Node with Intelliducer Plugs**

On the morning of the load test, the BDI wire leads were retrieved from under the bridge and connected to the wireless BDI nodes, which were in turn connected to the wireless base station, which communicated wirelessly with the computer controlling the system. In addition, pre-made cardboard shields or “igloos” (Figure 17) were mounted to protect the externally mounted strain gauges from wind, as other researchers have noted that BDI strain gauges tended to have a sensitivity to wind currents.



**Figure 17. Cardboard Shield (“Igloo”)**

Along with the BDI system, the lead wires from the internally mounted VWGs were connected to the appropriate CSI datalogger for periodic measurements. For live load testing it was necessary to disconnect 15 pre-select gauges to be measured dynamically and set up the dynamic CSI system (CR3000). For the VWGs remaining on the “static” datalogger system (CR1000), the measurement and recording frequency was limited due to the speed of the datalogger and required about a minute to cycle through all of the gauges sequentially. Therefore, the load truck was parked at predetermined locations during the third run of each test to allow the “static” datalogger sufficient time to acquire the measurements.

In addition to the instrumentation on the bridge, a BDI product called an *Autoclicker* was attached to the wheel well of the load test truck to track the time and longitudinal position of the truck as it crossed the bridge (Figure 18). Prior to testing with a particular vehicle, the research team measured the distance traveled during one complete revolution of the front wheels, or one “click” of the *Autoclicker*. A vice grip with a reflective paddle was attached to the wheel rim and a lens on a flexible arm was positioned over the paddle such that each time the wheel made a complete rotation, the *Autoclicker* would recognize the paddle and provide a “click” or instantaneous, time-stamped unit value. Using the geometry of the truck, the relative progress for each of the axles is illustrated versus the number of clicks in Figure 19. Each time the truck pulled up to the start of the bridge deck, the reflective clicker tab would manually be reset to the “zero” position on the wheel, where the *Autoclicker* would clock a click near the start of the truck motion.



Figure 18. BDI Autoclicker Setup

## Load Testing

The load test was performed on the afternoon of August 6 by driving the load vehicle East to West across the bridge at predetermined transverse positions as shown in Figure 15. The load trucks that were used were VDOT tandem-axle dump trucks loaded with gravel (Table 2). Truck RO6187 was used for the static test configurations while Truck RO9185 was used for the dynamic tests. The change in truck between the two sets of tests was necessary due to a damaged grease socket on the driver’s side front wheel that occurred at the end of the static testing program.

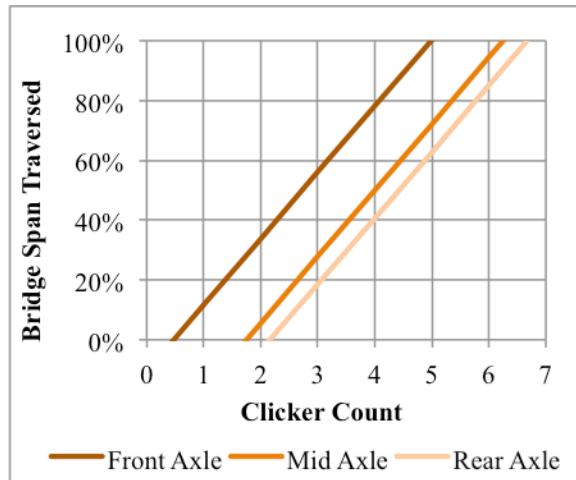


Figure 19. Autoclicker Position Encoder

Table 2. Load Test Truck Specifications

Truck Configuration/Position	Truck RO6187 (Quasi-Static)	Truck RO9185 (Dynamic)
Front Axle Weight	18.12 kip	17.32 kip
Rear Axle Weight	33.98 kip	33.20 kip
Total Truck Weight	52.10 kip	50.52 kip
Front Axle Width (center-to-center of tires)	82 in	79 in
Rear Axle Width (center-to-center of tires)	73 in	73 in
Tire Width	10 in	10 in
Front Axle Span	165 in	162 in
Rear Axle Span	53 in	55 in
Single Tire Rotation Travel Distance	129 in	--

### Static Testing

During static testing, the truck was positioned in each of the eight different transverse locations in order to elicit a maximum response from each of the eight girders. In each scenario, the truck driver was guided (Figure 20) to ensure that passenger’s side wheel path aligned with the designated paths marked on the bridge deck and proceeded along the bridge at an idle speed that was less than 5 mph. Thus, much of the static testing was more quasi-static in nature. Those data for the static testing were captured at 25 Hz for the BDI system and 100 Hz for the CSI dynamic system; the CSI dynamic system also recorded a separate dataset at 1 Hz. Each transverse run was performed a total of three times, where the third run was paused for 60 seconds close to the midspan of the girder nearest the driver’s side wheel path. This pause was intended to allow the remaining non-dynamically monitored VWGs to collect a true static picture of the loaded configuration. These static tests provided critical information regarding the system-level load sharing behavior as well as internal composite load sharing behavior of the HCB system.

The initial plan included additional static tests with a dual truck loading configuration; however, the RO6187 had to return to the shop due to the aforementioned damaged grease socket. As a result, the dual truck loading configuration was not performed. Furthermore, the



**Figure 20. Static Load Testing with Truck Guided Along Wheel Path A**

testing was progressing into the later part of the day and the team wanted to ensure the dynamic testing was performed prior to a large increase in traffic across the bridge.

### *Dynamic Testing*

As the heavier truck had left the site for repairs, truck RO9185 was used for the dynamic testing. A series of baseline static test runs were performed with this truck to provide a reference for the dynamic measurement. The load configurations for the baseline and dynamic testing were limited to positions B and D (Figure 15); these positions were selected because of the ease of traveling at the posted speed limit and maintaining the proper travel path. Traversing the bridge in the eastbound lane at the posted speed limit was not possible due to the curvature of the approach roadway. For ease of navigation, the wheel path lines marked on the bridge were adjusted to allow the driver to follow the path along the driver's line of sight rather than the passenger's wheel line. At each of the two locations, 2-3 dynamic runs were performed near the posted speed limit (between 35-45 mph). During the dynamic load testing, the data were captured at 200 Hz for the BDI system and 100 Hz for the CSI dynamic system.

## **RESULTS AND DISCUSSION**

Following the completion of the load-testing program, the data were retrieved from the data acquisition systems and post-processed by the research team. Upon retrieval of the data, it became apparent that a number of holes existed in the collected datasets, primarily within data collected using the long-term monitoring system CSI DAQ (CR 1000/AWV200/AM32B). Unfortunately, this system was not successfully deployed during the load testing, and, as a result, none of the data from the secondary sensors was collected during the parked loading scenarios

for each load configuration. In addition, the dynamic CSI DAQ (CR 3000/SC-CPI/CDM-VW305) had limited memory and ended up overwriting data collected during the load testing. However, while the dynamic data were not collected with this system, the internal gauges connected to the dynamic system were interrogated at a frequency of 1 Hz, which allowed for part of the static data to be salvaged. Processing the available data, the following behavior characteristics were evaluated:

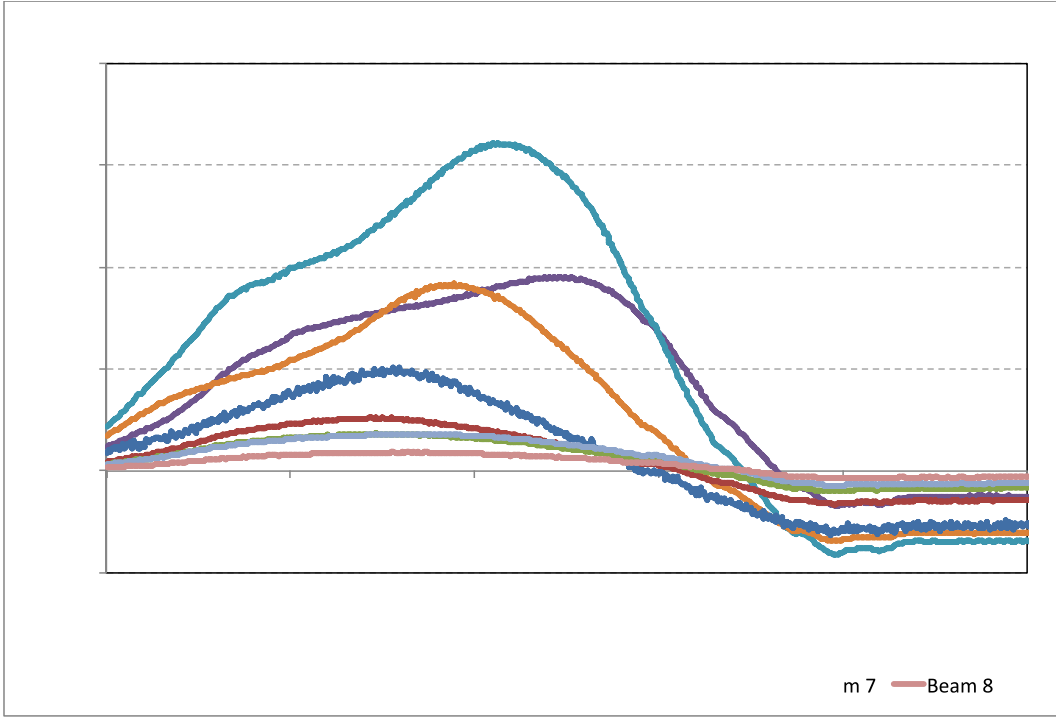
- Lateral Load Distribution – a phenomenon that describes the transverse load sharing behavior of a beam bridge system and a fractional measure of how much load is resisted by an individual member. The fractional representation is generally considered a simplification of complex two-way bridge system interactions down to a one-way behavior representation and is typically used for member design.
- Internal/External Load Sharing Behavior – the relative load sharing behavior for the HCB system that describes the relative contribution of the internal (concrete arch and prestressing steel) and external (FRP shell) components.
- Dynamic Load Allowance – the amplification of load above that of the static loading that occurs during dynamic loading. This phenomenon is typically described as a function of the interaction of the bridge and vehicle dynamic response interaction and is influenced by properties such as mass, stiffness, vehicle speed, and surface roughness.

### **Flexural Lateral Load Distribution Behavior**

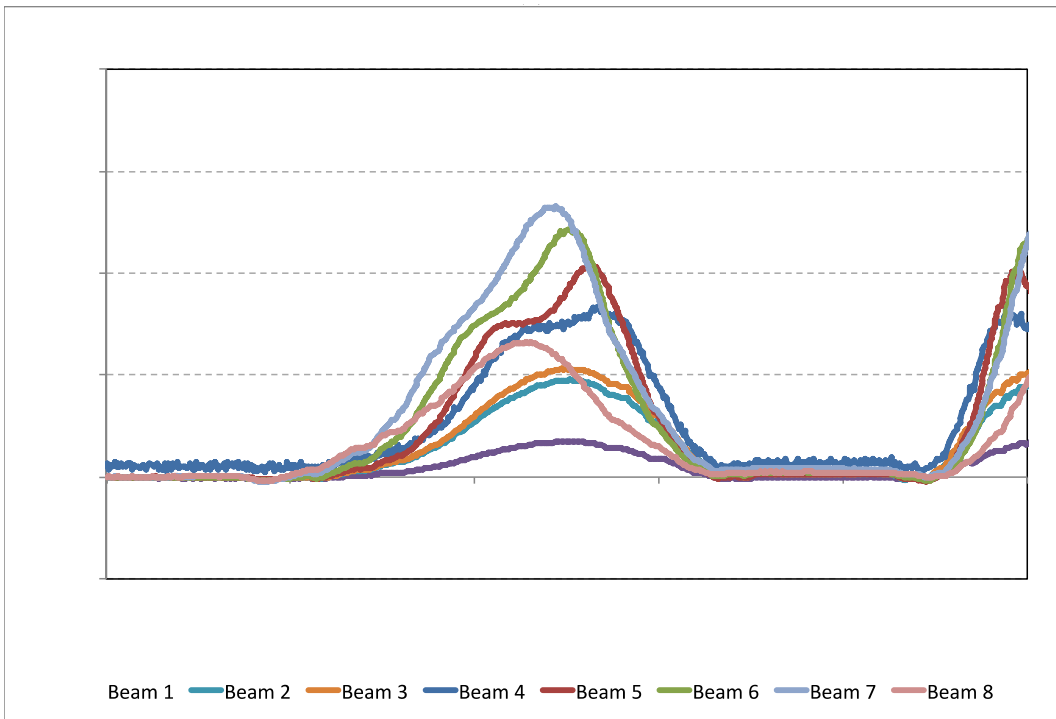
In this study, the flexural lateral load distribution behavior was analyzed to help evaluate the in-service behavior of the HCB bridge because such in-situ performance is critical to the end user, yet there is very little data available in this regard. Within a typical beam bridge structure, the expected behavior under load is that the girders most directly under the loading will resist the majority of the load, with the girders further away resisting less. This phenomenon is illustrated in Figure 21 which presents the select time series strain data for Load Case A (Run 1) and Load Case F (Run 1). For the Load Case A, Beam 2, which is straddled by the load truck, clearly experiences the greatest amount of strain with lower magnitudes of strain observed in the two adjacent beams (Beams 1 and 3). It is interesting to note that Girder 1 would be expected to also have sizable response, but this effect is somewhat muted by the influence of the parapet. A similar response is observed for Load Case F, where Beam 7 exhibited the largest strain response relative to the adjacent beams.

The lateral load distribution behavior is known to be influenced by a number of factors including girder spacing, deck thickness, span length, and girder stiffness. Using the time of occurrence of the maximum strain within the most heavily loaded beam as the point of reference, the load sharing phenomenon for various load cases is illustrated in Figure 22 through Figure 29.

As previously highlighted, the most heavily loaded girders experience the greatest bottom flange strain and internal strain, while girders further away experience less. An interesting phenomenon observed through these strain profiles is the contribution provided by the parapet



(a)



(b)

Figure 21. Time Series Strain Data (All Beams) – Static Loading (a) Load Case A1 and (b) Load Case F1

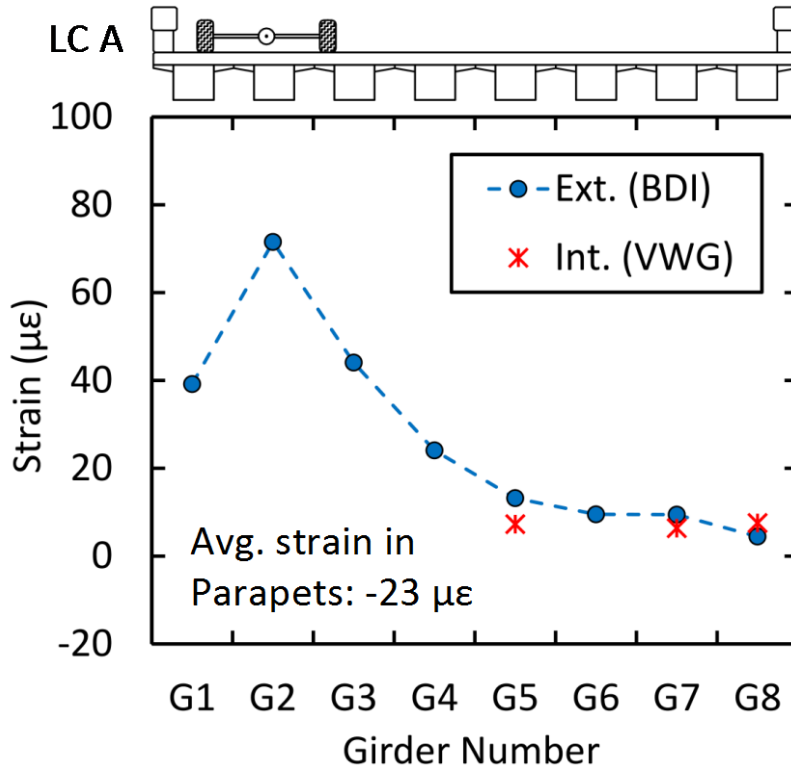


Figure 22. Tensile Zone Strain Across Cross-section (LC A)

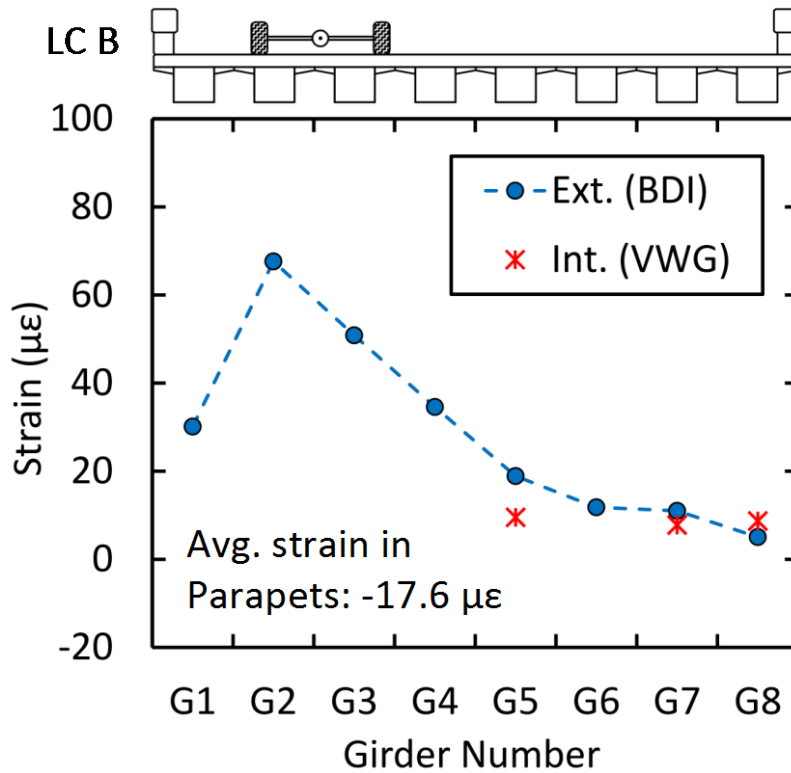


Figure 23. Tensile Zone Strain Across Cross-section (LC B)

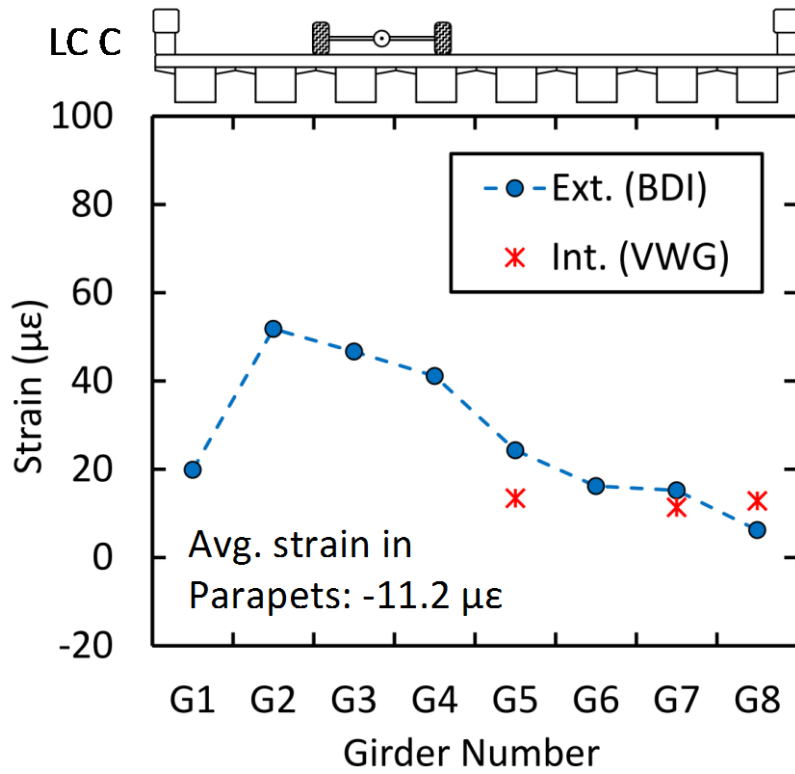


Figure 24. Tensile Zone Strain Across Cross-section (LC C)

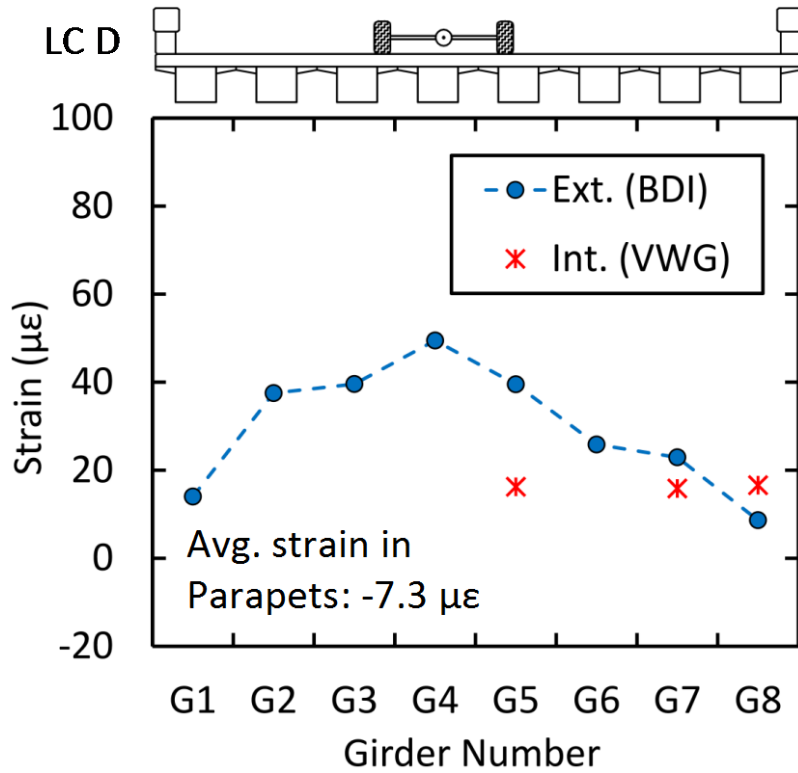


Figure 25. Tensile Zone Strain Across Cross-section (LC D)

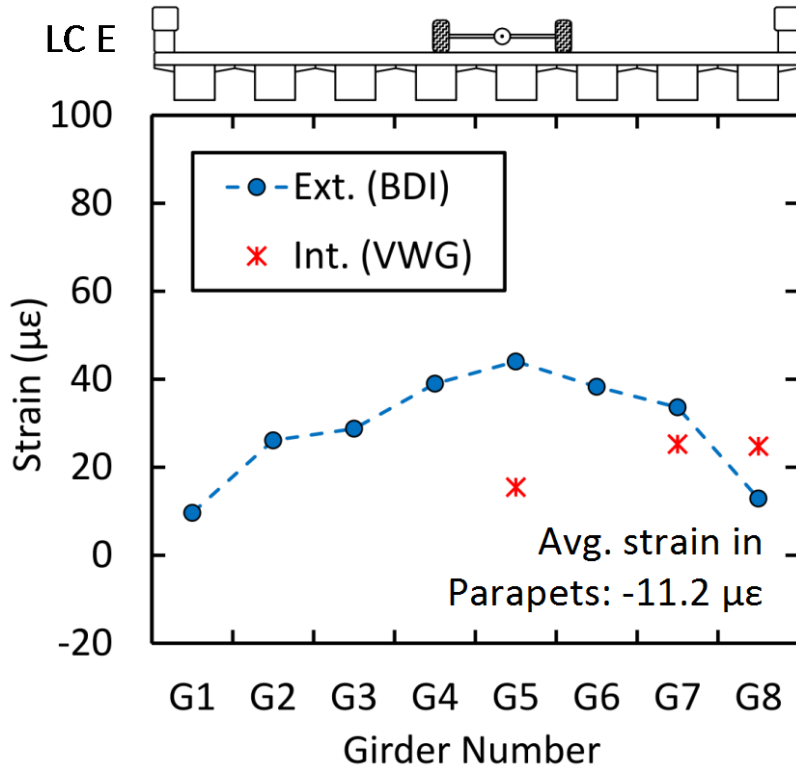


Figure 26. Tensile Zone Strain Across Cross-section (LC E)

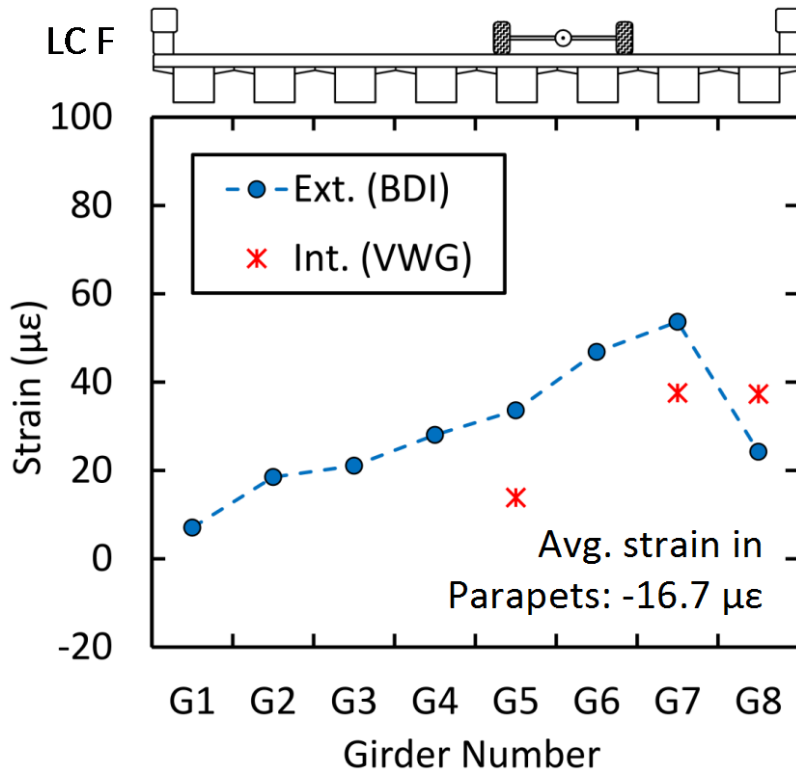


Figure 27. Tensile Zone Strain Across Cross-section (LC F)

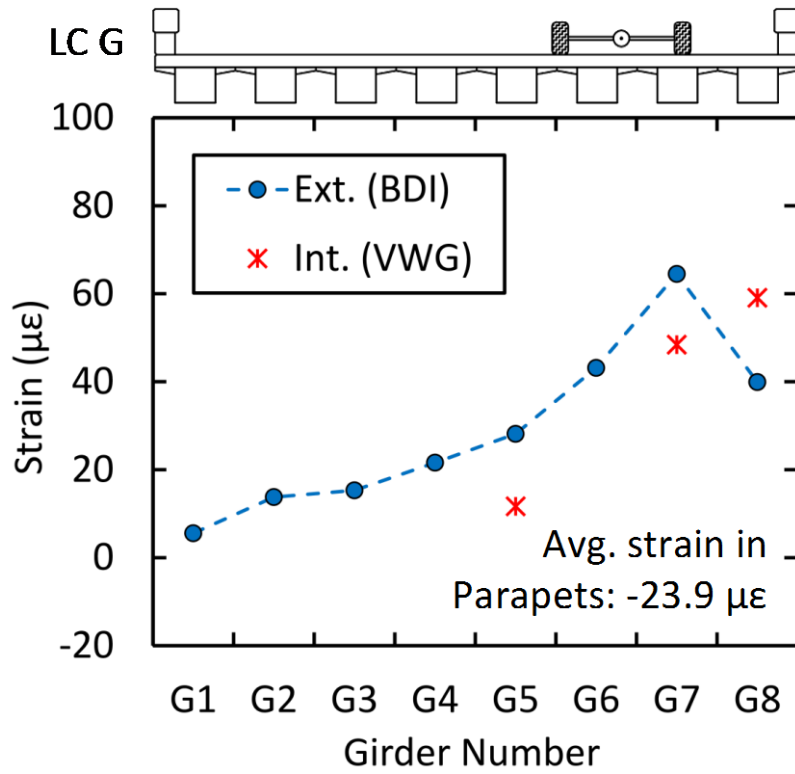


Figure 28. Tensile Zone Strain Across Cross-section (LC G)

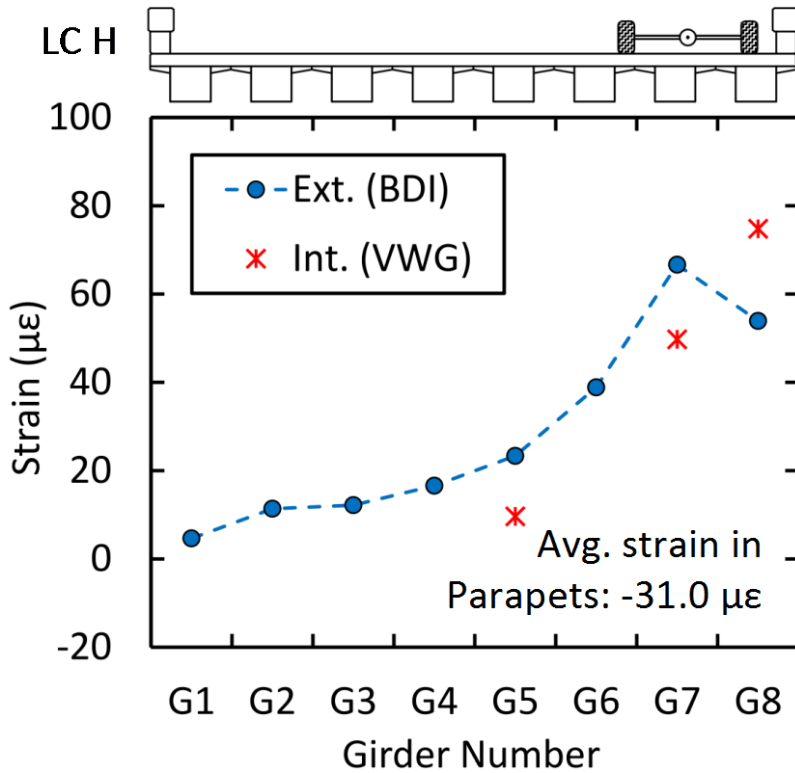


Figure 29. Tensile Zone Strain Across Cross-section (LC H)

wall, which carry a fraction of the load, as evidenced by the decrease in strain in the exterior beams. In the Virginia Tech study, Ahsan (2012) observed a similar distribution response for the interior girder, but the exterior stiffening effects were not present due to the lack of parapets in those tests. It should also be noted that this phenomenon was not observed in the internal VWGs, likely due to the non-composite behavior between the internal and external beam components.

When comparing the strains observed on the exterior (BDI) with those measured internally (VWG), the VWG strains do not consistently match the same trend for lateral load distribution. The internal strain readings are consistently lower than the external FRP strains, with the exception of the fascia girder number 8. The cause of this non-correspondence is unknown, but may be attributed to the non-composite behavior of the HCB components, as discussed in the next section on element load sharing behavior. This non-composite behavior theory is also reinforced by an observation of the strains near the exterior of the bridge near the parapet walls where there is a lower stiffening effect on the internal tension strands than the FRP shell.

The lateral load distribution response, as previously defined, describes the relative load fraction resisted by each girder within the system. Equation 1 is commonly used to describe the flexural lateral load distribution response (Eom and Nowak, 2001; Waldron et al., 2005; Harris et al., 2008; Harris, 2010), where strains at mid-span are the measured inputs. Using this relationship, the average maximum distribution factors for each of the load configurations are summarized in Table 3. The values presented in the table include the controlling or maximum distribution factors for both the interior and exterior girder locations as described by AASHTO (2012) and are aligned with the measured response of the most heavily loaded beam for each load case. Also included are the calculated flexural distribution factors from the AASHTO LRFD Bridge Design Specifications (2012) for the cases of conventional slab-girder bridge system such as a concrete deck on reinforced concrete girders (AASHTO Type A) or a concrete deck on box girders (AASHTO Type B), as well as the calculated values from the historical AASHTO Standard Specification (2002). Results from the three-girder HCB system tested at Virginia Tech (Ahsan, 2012) are also included for reference.

$$DF_i = \frac{\epsilon_{\max i}}{\sum_{i=1}^{\# \text{ girders}} \epsilon_{\max i}} \cdot (\# \text{ of Trucks}) \quad \text{Eq. 1}$$

For the load-testing program, the controlling distribution factor for the interior girder resulted from Load Case A, while the controlling value for the exterior girder occurred for Load Case H. This exterior girder response highlighted the effect of the skewed configuration on the lateral load distribution behavior of the system. Despite the almost symmetric loading conditions (A compared to H) and symmetric cross section of the bridge, the skew caused the exterior girder to behave differently on opposite sides of the bridge, with lower exterior distribution factors measured for Load Case A. The interior distribution factors from the field test were slightly lower than the results from the study by Ahsan (2012), indicating a more uniform load sharing phenomenon than was found in the full-scale laboratory testing. This is not surprising considering the Tides Mill Stream Bridge had more beams amongst which to distribute the load. Furthermore, the measured exterior distribution factors were lower than the laboratory values, most likely due to the absence of the parapet walls in the preliminary study.

**Table 3. Summary of Mid-span Flexural Distribution Factors**

Configuration Scenario	Max. Exterior	Max. Interior
Load Test Results		
Load Case A	0.188	0.349
Load Case B	0.135	0.316
Load Case C	0.094	0.256
Load Case D	0.059	0.220
Load Case E	0.051	0.199
Load Case F	0.103	0.230
Load Case G	0.164	0.281
Load Case H	0.225	0.298
<b>Controlling</b>	<b>0.225</b>	<b>0.349</b>
AASHTO LRFD		
Cast-in-place concrete deck on steel or concrete beams (Case A)	0.247	0.360
Cast-in-place concrete deck on closed steel or precast boxes (Case B)	0.288	0.306
AASHTO Standard Specification	0.371	0.371
Virginia Tech (Ahsan, 2012)	0.390	0.360

When comparing the field test results to the AASHTO provisions, it should be emphasized that the AASHTO LRFD and the AASHTO Standard Specifications do not contain provisions for the HCB system. Nonetheless, the anticipated HCB element behavior was something similar to that of a conventional slab-girder bridge system such as a concrete deck on reinforced concrete girders (AASHTO Type A) or a concrete deck on box girders (AASHTO Type B). Even when accounting for code-specified adjustments for skew, the Type A and Type B designations yielded conservative estimates for the exterior girders compared to the experimental results. On the other hand, only the Type A design value was conservative for the interior distribution factor.

In contrast, the quarter-span location did not mimic the distribution responses at midspan. The quarter-span location exhibited some degree of counter-flexure, which was likely the result of a combination of plate action of the bridge system, skew, and boundary conditions. These results are not presented herein, but can be found in Civitillo (2014). However, the internal VWGs at the quarter spans did track the external strains much more closely than at the mid-span locations. While the internal strains still tended to be slightly lower than the external values, the discrepancy between the two gauges was seldom more than a few microstrain, suggesting that there was not as much slippage between the internal steel and external FRP shell. The reason for the difference in behavior at the two span locations is also unknown, as the load carrying elements were self-contained within the shell and not readily available for inspection. However, one possible theory is that the tension steel pulled away from the FRP shell at midspan because of the lack of support provided by the foam. In other words, as curvature developed in the beam during flexure, the tension steel may have pulled away from the FRP shell and remained as linear as possible in tension, while the curvature of the bottom flange of the FRP was enforced by the stiffness of the side webs tying into the remainder of the system and the curvature of the deck. A simplified diagram depicts this phenomenon in Figure 30; the dashed line represents the deflected beam shape. The solid line represents the tensile steel that may not follow the curvature of the beam due to lack of restraint. While the steel is embedded in the FRP, it is not restrained above by anything but a single layer of FRP and foam. A single extreme loading event may be enough to separate the steel from the FRP, and each subsequent loading would

exhibit this effect. Such a phenomenon would surely be accentuated at mid-span, where curvature of a traditional beam is maximized.

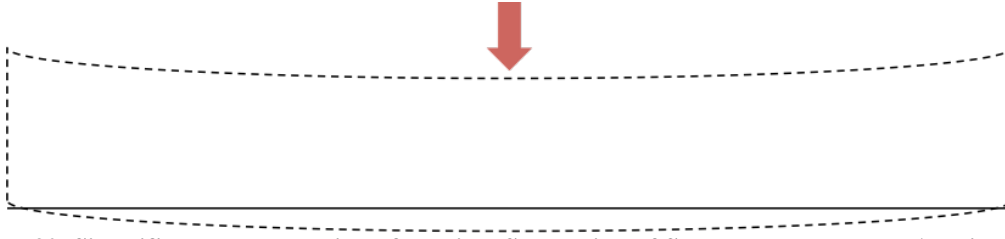


**Figure 30. Simplified Representation of Possible Separation of Steel and FRP Under Applied Load**

### **Element Load Sharing Behavior**

The HCB system is a composite system that is constructed in multiple stages and as a result, characterization of the internal element level load sharing behavior is critical. An understanding of this internal load sharing behavior is also essential for maintenance and decision-making processes as the system ages. The internal (VWG) and external (BDI) instrumentation allowed for the measurement of the strain profile through the depth of girders 5, 7, and 8 during loading. The data provided critical information on the load sharing behavior between the concrete arch, FRP shell, and reinforcing steel, as well as the location of the neutral axis of the composite cross-section. One critical note is that while the HCB is designed as a tied arch system, once the deck is cast, the neutral axis occurs in the deck. Thus, the entire HCB, including the arch, can be expected to be in tension, including the arch, at mid-span under superimposed dead load (Van Nosedall et al., 2013).

Figure 31 through Figure 34 illustrate the midspan strain profiles through the depth of the cross-section for beams 5, 7, and 8 subjected to Load Cases A, F, G, and H. Load Case A is presented merely for illustrative purposes, while Load Cases F, G, and H were selected because the load truck was in close proximity to the three girders that maintained both internal and external instrumentation through the depth of the beams, and thus yielded the most relevant results pertaining to the composite behavior of the HCB. The transition from positive strain at the tension steel to negative strain within the deck defined the location of the neutral axis, i.e. zero strain. The occurrence of the neutral axis varied for each of the load cases and it was difficult to define a consistent neutral axis location because the profile through the depth was not linear as might be expected for the design assumption of full composite action. As an example, the tensile strains in the arch section of Girder 5 exceeded those in the tensile strand level. At first it was surmised that the higher concentrations of strain were due to service load tensile cracking in the unreinforced arch concrete, solely intended for support during construction (Van Nosedall et al., 2013). However, after evaluation of the quarter-span strain profiles (Figure 35 through Figure 38), it appears that the two steel strands resting along the bottom of the arch profile, which were used to anchor the stirrups, may be carry significant levels of tension, despite their absence in design calculations. The VWG arch strains seen in the quarter-span plots (Figure 27) are in tension, well beyond the cracking strain of the arch concrete, yet the arch continues to carry the strain. Another potential source of this discrepancy in the neutral axis location is the occurrence of slip between the concrete deck and the HCBs; however, this phenomenon could not be discerned from the available data.

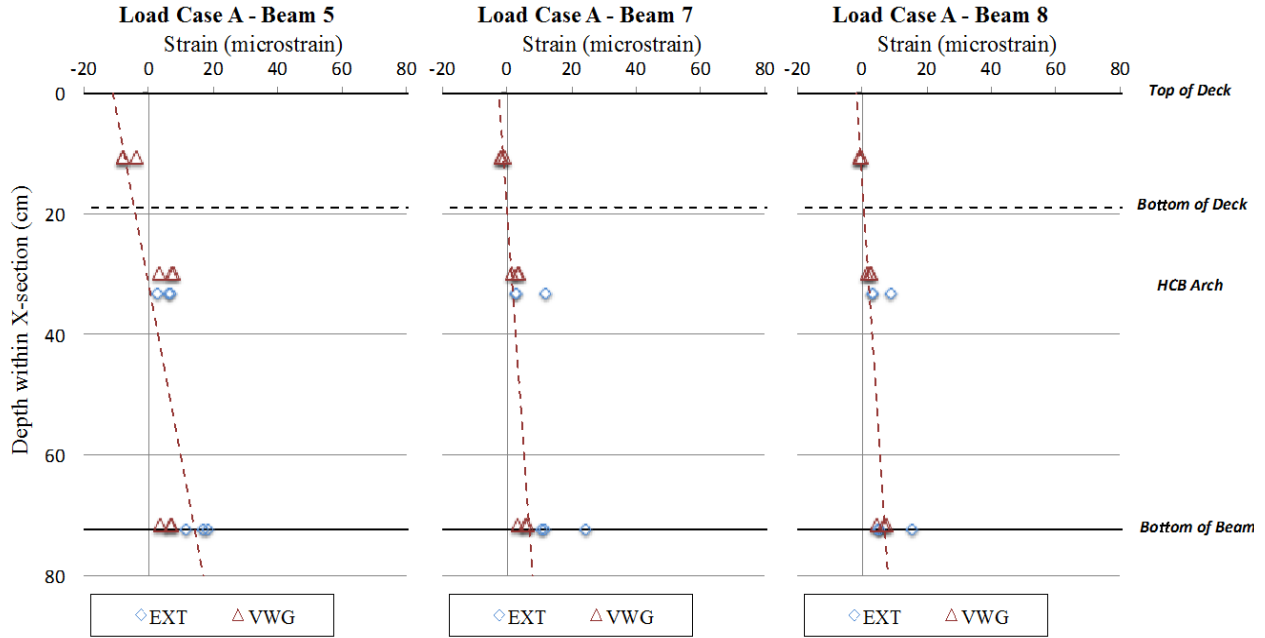


Figure 31. Mid-span Strain Profiles Load Case A

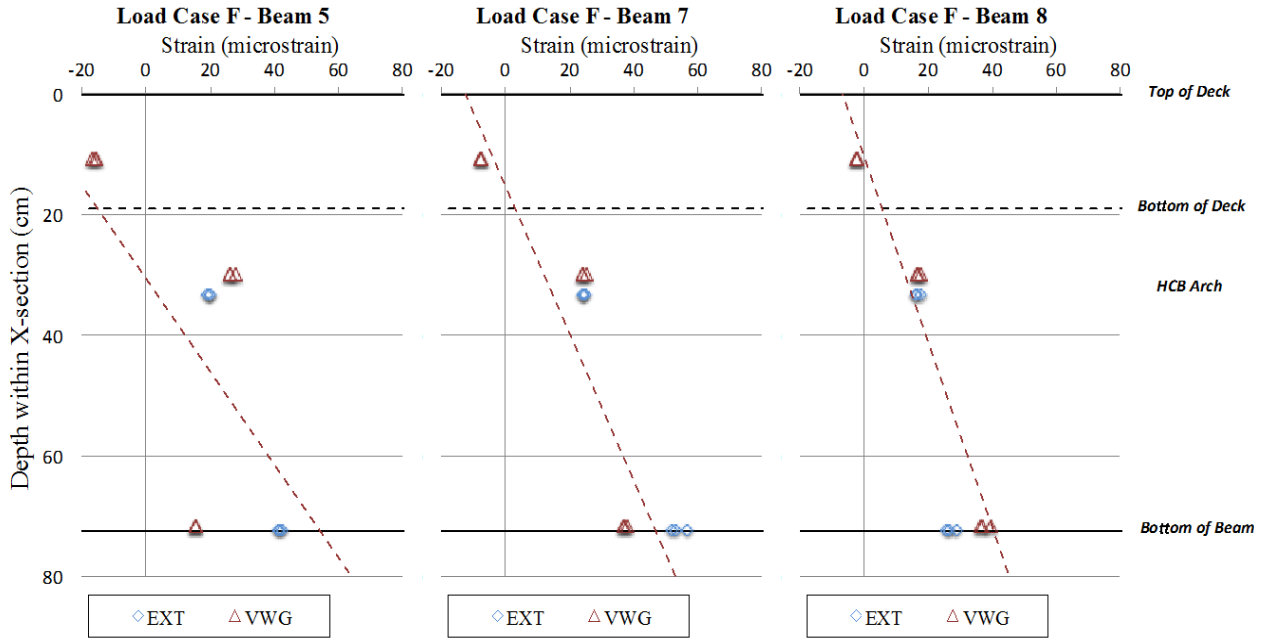


Figure 32. Mid-span Strain Profiles Load Case F

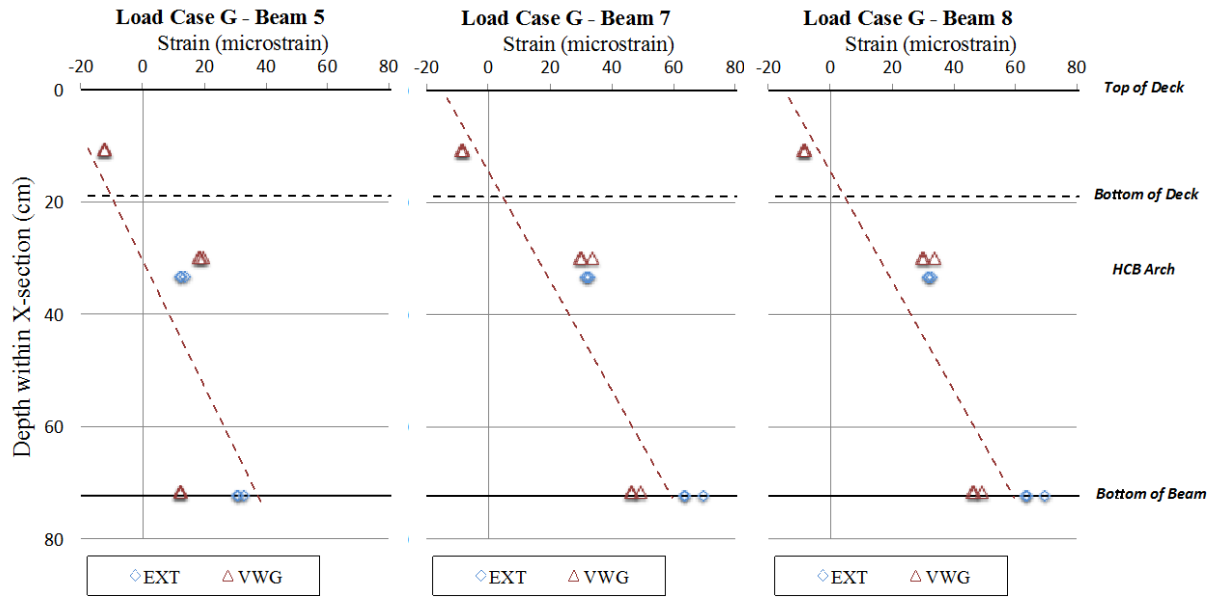


Figure 33. Mid-span Strain Profiles Load Case G

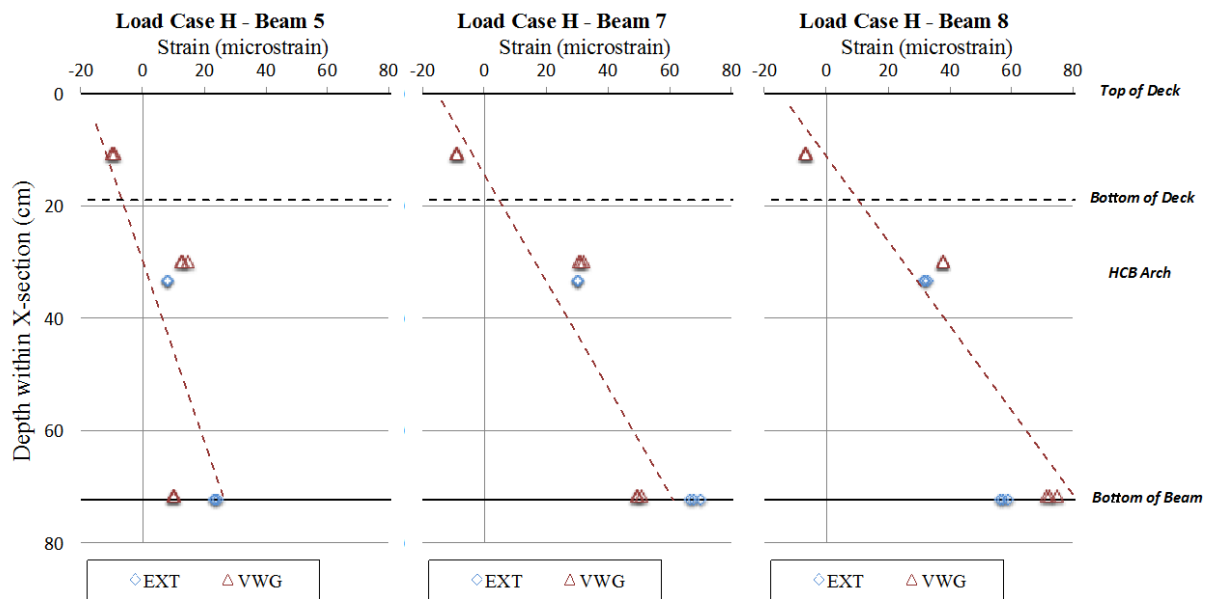


Figure 34. Mid-span Strain Profiles Load Case H

Rather than cracking in the arch, Ahsan (2012) hypothesized that there exists a local bending phenomenon within the concrete arch. As illustrated in Figure 3, it can be rationalized that the arch would be able to experience bending, especially at higher levels of overall HCB curvature where the arch begins to flatten out. Ahsan also proposed that this effect is dampened at mid-span due to the 8 ft sheet of FRP that serves as the bottom formwork for the arch, which also likely provides stiffening to the arch. This FRP sheet that forms an enclosure for the arch at this location also connects to either FRP web and thus enforces greater congruence with the FRP curvature and overall HCB response at mid-span. The data collected in this experimental program aligned with the hypothesis, as the quarter-span arch gauges of Beams 5 and 7

experienced uncharacteristically high levels of tensile strain, often greater than the maximum tensile strain in the bottom flange of mid-span girders. Beam 8 did not exhibit such an accentuated trend, but this was likely caused by the stiffening effect of the parapet in combination with the additional steel (nearly double that in the interior girders) added to the tension zone of the exterior girders. These exterior beams were likely stiff enough to minimize beam curvature, and the local bending effects in the arch were therefore not as evident.

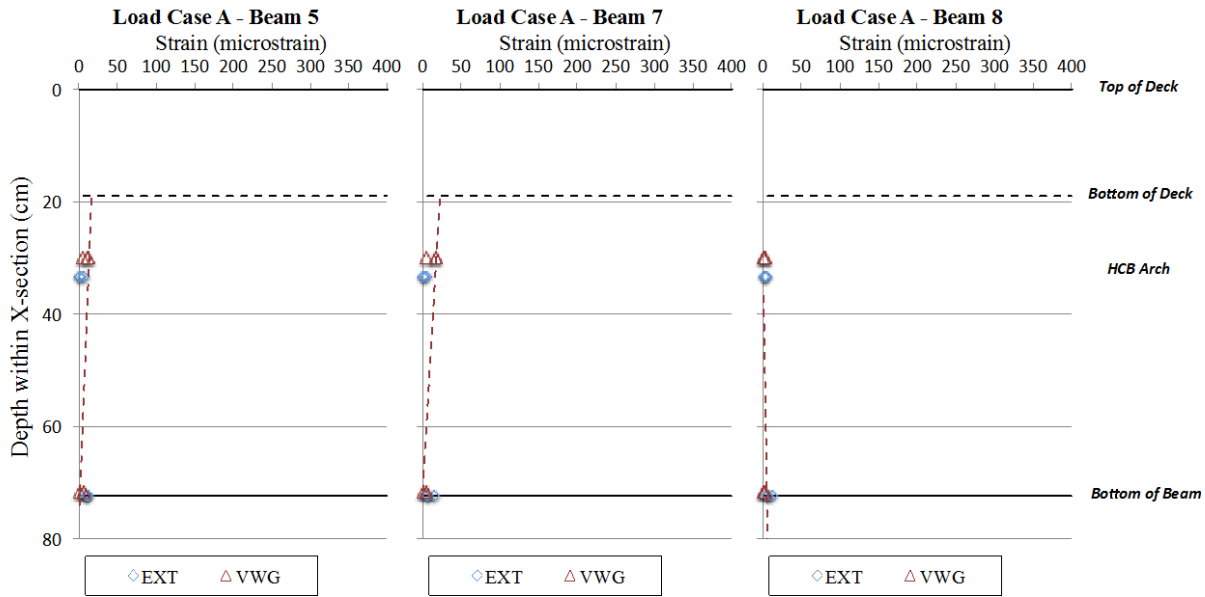


Figure 35. Quarter-span Strain Profiles Load Case A

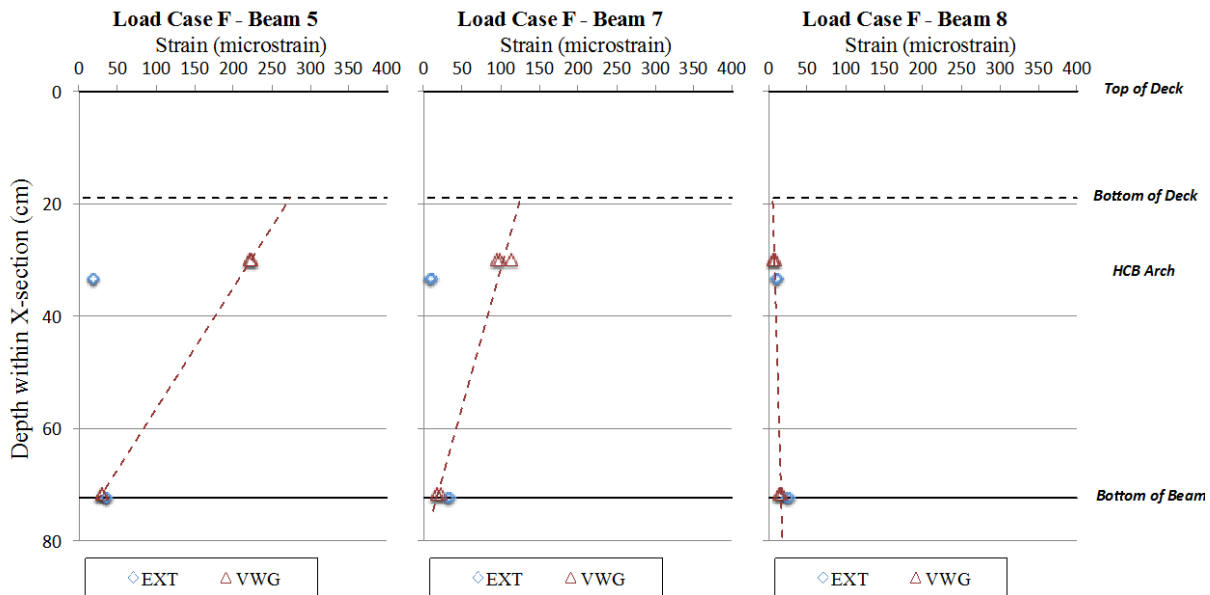


Figure 36. Quarter-span Strain Profiles Load Case F

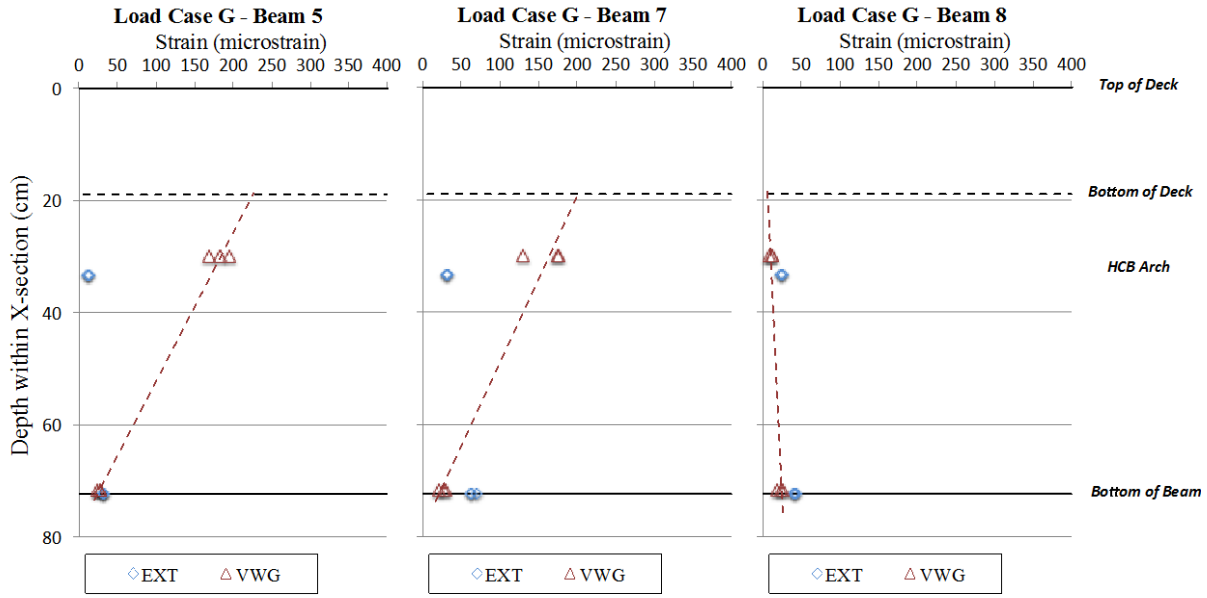


Figure 37. Quarter-span Strain Profiles Load Case G

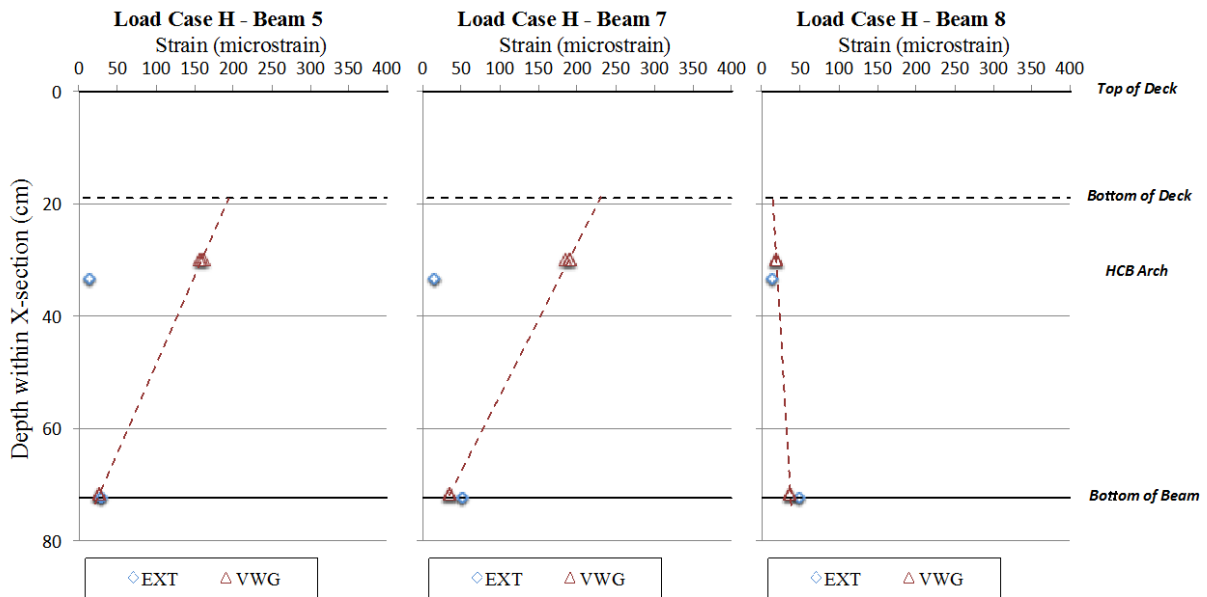


Figure 38. Quarter-span Strain Profiles Load Case H

### Dynamic Load Allowance

As described in a previous section, the dynamic load allowance (DLA) or impact factor accounts for the amplification of the design static live load due to a moving vehicle crossing a bridge. The dynamic response of HCB was of particular interest in this investigation because of the lightweight of a typical HCB versus a conventional steel or concrete beam. In addition, the design of this system was controlled by deflection and the dynamic response can be related to the inherent flexibility of the system.

To study this behavior, load test results from a static load case and a series of corresponding dynamic load tests were used to determine the dynamic load allowance. As described in the experimental program, the testing was limited to Load Cases B and D to allow the loading truck to traverse the structure near the posted speed limit. Using the relationship presented in Equation 2, the dynamic load allowance, represented as a percent increase, was determined as the additional response observed under dynamic loading conditions relative to the corresponding static response. A representation of this additional dynamic response is presented in Figure 39 from the superposition of strains observed during the static and dynamic tests. All of the measurements for the dynamic response were derived from the externally mounted BDI gauges on the tension side of the HCB beams. The original test plan included plans to measure the VWGs dynamically; however, this effort proved unsuccessful, so only the external gauge measurements were recorded and used in this analysis.

$$DLA = \frac{\epsilon_{\text{dynamic}} - \epsilon_{\text{static}}}{\epsilon_{\text{static}}} \cdot 100\% \quad \text{Eq. 2}$$

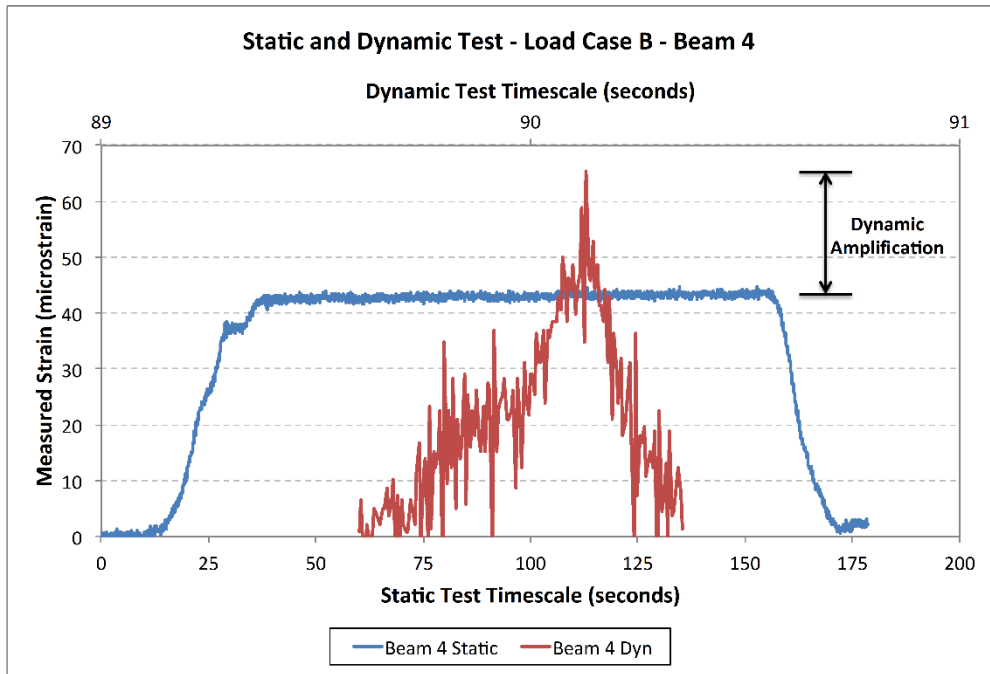
The controlling or maximum dynamic amplification response for each of the two load truck positions tested under dynamic conditions is presented in Table 4 along with the design values from the AASHTO LRFD and Standard Specification (AASHTO, 2002; AASHTO, 2012). These measured values represent the amplification observed in the most heavily loaded girders for the respective load cases. The table shows that the average dynamic amplification was comparable to those prescribed by AASHTO, but there is the potential for larger amplification as demonstrated by the maximum responses observed in the most heavily loaded girders, as much as 46% compared to the AASHTO LRFD value of 33%. In the maximum dynamic amplification cases shown, the maximum response registered in Beam 4 for Load Case B was 46%, while a response of 33% was registered in Beam 7 for load case D.

**Table 4. Summary of Dynamic Load Allowance**

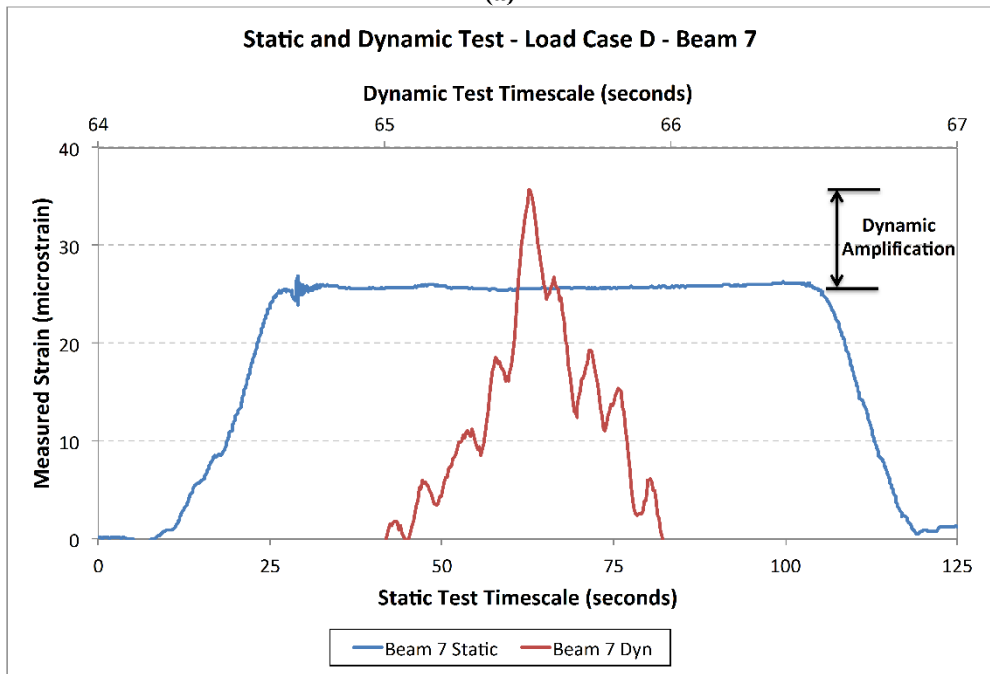
<b>Configuration Scenario</b>	<b>Max. DLA</b>	<b>Girder with Max. Response</b>
<b>Load Case B</b>		
Run B1 – Tested at 35 mph	46%	Beam 4
Run B2 – Tested at 40 mph	43%	Beam 4
<b>Load Case D</b>		
Run D1 – Tested at 40 mph	31%	Beam 7
Run D2 – Tested at 45 mph	33%	Beam 7
<i>Measured Average</i>	23%	-
<b>AASHTO</b>		
LRFD	33%	-
Standard Specification	30%	-

### **Evaluation of Long-Term Inspection Techniques**

Due to the nature of being a new structural system in the well-established field of bridge engineering, there is a lack of experience for inspection of the HCBs, especially when considering the encasement of the critical load-bearing elements of the system. These components are not readily available for visual inspection, so the following section presents a



(a)



(b)

Figure 39. Maximum Dynamic Amplification Response (a) Load Case B and (b) Load Case D

summary of NDE techniques and their feasibility for accomplishing specific inspection tasks. This evaluation was limited to a literature evaluation, and none of the proposed methods has been tested. The summary of techniques and discussion is presented as a progression through the depth of the cross-section, beginning with the deck and working down to the beam level, which is divided into internal and external components. It should be noted that a study on the durability

of HCB components was recently initiated at the Virginia Transportation Research Council and the results of this investigation will be available in a separate report upon completion.

### **Reinforced Concrete Deck Inspection**

The 7.5-in concrete slab deck was reinforced according to traditional VDOT design practices. Thus, it does not vary significantly from a conventional reinforced concrete slab-on-girder bridge. Therefore, conventional concrete deck inspection methods apply here and will not be discussed in depth, but one should consider the methods that follow.

#### *Visual Inspection*

Visual inspection is an effective and economical method for investigating large deck surfaces quickly and economically. This type of investigation is effective in identifying significant surface defects that include, but are not limited to cracking, localized depressions and staining. While only surface defects may be detected, taking note of their characteristics may be indicative of internal concrete conditions and that of embedded rebar. Rust staining, for instance, is a good indicator of deterioration of internal steel. A visual inspection should include the orientation, width and if possible, depth of cracks (International Atomic Energy Agency, 2002). One strong advantage of visual inspection is the associated low cost associated. Typically, only very basic tools are required, unless access becomes a problem and heavy equipment is needed to provide an inspector a vantage point to capture the condition of the whole deck. Another consideration to be made when relying on visual inspection is the subjectivity of the inspectors. Each inspector may not have the same visual acuity for detecting small cracks, and one inspector may rate surface defects to be more or less critical based on their background. For this reason, it is important to use as many standardized forms of measurement as possible to quantify the deterioration. Visual inspection is also a good way to identify problem areas that can be inspected further with localized NDE methods.

#### *Ground Penetrating Radar (GPR)*

The inspection method of ground penetrating radar (GPR) is one of the more popular NDE methods for investigating the location and condition of embedded steel. GPR uses a near-field investigation of electromagnetic (EM) waves that have a wavelength greater than concrete aggregates and therefore pass through the non-homogenous material with ease. These waves interact with boundaries that have disparate dielectric constants and the reflections and refractions are recorded and analyzed.

Concrete attenuates these EM waves after a depth of about 2ft, making GPR ideal for concrete deck interrogation. Units have been manufactured that allow automation of the process, making short work of B-scans, and even three-dimensional C-scans. Successful applications have been developed where an array of GPR units mounted on a vehicle moving at highway speeds collect data from a bridge deck. One drawback is that this method is on the expensive side of the NDE inspection methods. Additionally, the dielectric disparity between concrete and steel is so high that the entire EM wave is reflected at these steel boundaries, therefore rendering the slab beneath these boundaries imperceptible (Geophysical Survey Systems Inc., 2006).

### *Impact Echo*

The mechanics of the impact echo (IE) inspection method rely on the interpretation of the response of stress waves produced by an impact. The theory behind impact echo testing is to impart a transient point impact that causes an elastic displacement wave throughout the material. This wave propagates spherically through the material and interacts with boundaries and interfaces causing reflections and transmissions depending on the acoustic impedance of the materials. The reflected signals will return to the surface and may be recorded. This method is ideal for detecting delamination, voids and honeycombing of a concrete deck. Impact echo is reliably accurate at detecting the location and depth of these sorts of defects. Impact echo is an efficient method when automated, but may be costly to implement (Sansalone, 1997).

### **Steel Strand Inspection**

As the high-strength steel strand is embedded within several layers of the glass FRP shell, it is not available for visual inspection, yet there is still a great interest in the condition of the steel just as would be the case with a conventional prestressed or reinforced concrete girder. Of particular interest with respect to the condition of the passive steel strand are the presence of any deterioration such as corrosion or yielding/breakage of the strands. Some of the methods that would be used to inspect steel embedded in concrete are applicable here; however, there are some key differences that may influence the evaluation using standard methods. For example, the steel in the HCB system is much closer to the exterior surface than traditional reinforced or prestressed concrete. In addition, the material properties of the FRP “cover” are different than those provided by traditional concrete cover. Highlighted in the following sections are a number of techniques that may be applicable for evaluating the condition of the internal reinforcement with the HCBs.

### *Magnetic Flux Leakage Inspection*

Magnetic flux leakage (MFL) provides a quantitative analysis of potential discontinuities of steel, that is, any reductions in cross-section or breaks in individual wires in a given strand. The benefit of this method is the ability of a magnetic field to penetrate materials that are not ferromagnetic, such as concrete or FRP. Magnetic flux leakage inspection involves saturating the ferromagnetic material, in this case high-strength steel, with a magnetic field that would flow longitudinally along a steel component that exhibits no defects or flaws. The theory behind the method is that any defects, be they cracks or loss of section due to corrosion, will cause a disturbance in the magnetic field, requiring that the magnetic flux detour around the defect. If the flaw is significant enough, the magnetic field will protrude beyond the boundaries of the steel, and in this case, even the FRP coating. Hall sensors are able to detect and quantify these deviations in the magnetic field (Figure 40). The method is able to detect very minute surface discontinuities that may be quantified in volume and depth. MFL has been used in a variety of applications and has been standardized.

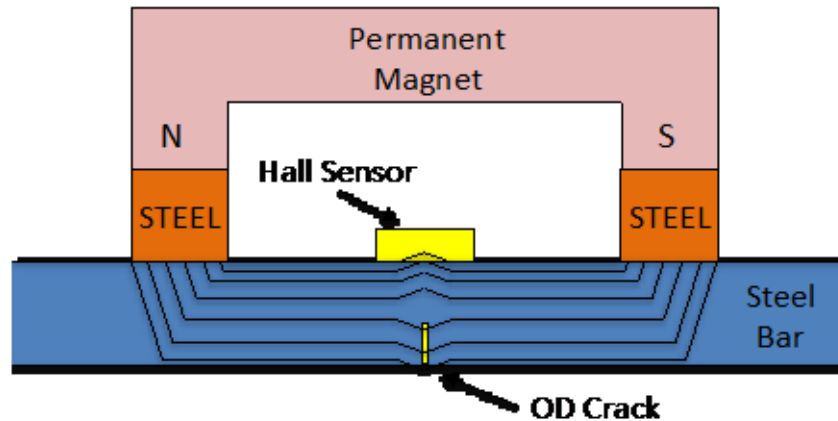


Figure 40. Magnetic Flux Leakage Theory. Adapted from Civitillo (2014).

However, the working clearance under this particular HCB application is limited by the low profile of the bridge over the tidal stream and the current tidal situation. One significant drawback to this method of inspection is the high relative cost of the equipment. This is mostly due to the difficulty of magnetically saturating larger quantities of steel. In the case of HCBs, the challenge would be finding a permanent magnet that could sufficiently and simultaneously saturate a large number of strands in close proximity, while also distinguishing between the individual strand responses. ASTM standards E570-09 (ASTM International, 2009) and STP371 (Committee A-6: Magnetic Testing, 1964) provide the inspection guidelines for effective implementation of this method.

### *Eddy Current Inspection*

The Eddy Current inspection method also provides quantitative data for discontinuities within steel and is similar to MFL in the use of electromagnetic theory for operation. Current is fed to a probe consisting of a coil of wire, therefore inducing a magnetic field around the probe. In the vicinity of a conductive object, the magnetic field generated by the probe will induce a current in the conductor. As a result, the current in the conductor will have its own magnetic field associated with it. The interaction between the two systems is known as mutual inductance, and changes in this inductance can be detected by the probe as a result of the dependence of the two systems. Differences in material properties and defects will cause a change in the current relative to a baseline reading, as well as the impedance in the test subject. However, as the readings are relative and dependent on several factors, the results may be challenging to interpret.

One important limitation to the eddy current method is the idea of liftoff. While magnetic fields are able to penetrate non-conductive materials such as FRP without inducing current, the strength of the signal produced by mutual inductance is diminished by the square of the distance. Although the thickness of the FRP is not great, any variance in the thickness of the resin matrix of the FRP at any location may register as a disparity that could easily be interpreted as a reduction in steel conductivity and thereby a defect at that location. Another important consideration is the restriction of this method to local investigations. As a single probe reading a single point in the plane of the bottom flange, it would take many hours and a lot of effort to take readings both longitudinally and transversely. Depending on the density of the readings, a large

portion of the steel could be easily neglected. The technology is, however, relatively inexpensive as compared to MFL inspection, and may be of use for local inspections of specific questionable areas as identified from visual inspection. Eddy current inspection is a fairly well established investigation method, and one should refer to the ISO 15549:2008 Eddy Current testing general principles standard (ISO, 2012).

### *Impact Echo/Mechanical Sounding*

While impact echo is ideal for concrete structures, it is also widely applicable to thin materials such as FRP. The reflections off the FRP/steel interface would provide a characteristic signal that would vary with the presence of corrosion or cracking. Just as in MFL inspection, a device may be designed with a position encoder to travel longitudinally along the beam and impart an impact at close intervals and record the response along the length. This design makes the method more attractive than a local inspection method such as eddy currents. The impact echo method has been standardized for use with concrete, and ASTM C1383 (2010) should be referenced.

### *Active Thermography*

Thermal investigations rely on the thermal emission of all materials at a temperature greater than 0 Kelvin. The cameras designed for this type of testing pick up the infrared signals that quantify the amount of heat energy radiating from a body at any given time. Each material exhibits its own thermal emissivity and thermal conductivity properties that make one material unique from the next. Thermography is often used to search for voids or delamination in concrete because the thermal properties of air are quite disparate from those of concrete. This type of NDE testing also has potential for evaluating delaminations in the FRP shell (Washer et al., 2013), which is presented in a later section.

As the high-strength steel strand and the FRP also have different thermal properties, an infrared camera should be able to pick up the thermal emissions of the steel through the thin layer of FRP. However, differentiating between individual strands may be difficult because the strands are spaced somewhat closely. Furthermore, section loss or deterioration will not be significantly evident as the thermal signals showing through the FRP will likely not be precise. For this reason, active thermography should be used by artificially heating one end of the beam's steel. As the strands heat up and creates a temperature differential over the length of the beam, the thermal conductivity of steel will allow heat to flow along the beam. This flow should be tracked over time. If any section loss or breakage of the strand has taken place, this would alter the rate of heat flow through the reduced cross-section, and the damaged strand could be identified relative to its neighbors. This method should also be able to identify the location of deterioration based on the spot in which the reduction in heat flow occurs. ASTM method D4788-03 (2007) is already established and provides the foundation for adopting thermography for use in HCB inspection.

### *Visual Inspection for Local FRP Bulging*

Corrosion products produced from steel degradation require more volume than pristine steel. So any significant corrosion of the steel internal to the FRP shell could potentially force the bottom layer of FRP outwards. Therefore, any local bulging or out-of-plane deformation observed in the bottom FRP flange during basic visual inspection of the HCBs should certainly be noted. Subtle bulges may not be evident to the naked eye, but using a straight edge can help with detection. Even imperfections that may have formed during the manufacturing process should be noted for future tracking and investigation using additional NDE methods. However, there is the possibility that these corrosion products may not be substantial enough to noticeably force the bottom layers of FRP outwards. There is only a single layer of FRP above the steel, followed by polyisocyanurate foam, which are collectively likely much less stiff than the lower FRP, and may be more likely to compress or deflect than the lower FRP. Until being investigated more thoroughly in a laboratory setting and being standardized for field inspection of HCB bridges, visual inspections should not be exclusively relied upon when determining the condition of the tension steel strands.

### **FRP Inspection**

The FRP shell was not originally considered to be a primary load-carrying component of the HCB; however, recent tests at Virginia Tech have shown that the shell does contribute to the shear resistance. In addition, the material is still of interest from a durability perspective as the shell provides protection for the interior system components from the surrounding environment and potential penetration of moisture, chlorides or other detrimental elements that may cause corrosion of the steel or deterioration of the concrete. While the FRP is expected to remain linearly elastic in the range of service loads, extreme loading events may cause micro-cracking of the shell that could lead to the FRP absorbing moisture. This potential penetration is disconcerting as the moisture and other contaminants would likely remain inside of the FRP and be in direct contact with the steel. In this regard, a major uncertainty that remains is that if these cracks were to form, would the cracks permeate to the depth of reinforcement and if so, how large a crack would be necessary to allow moisture to reach strand. Other than cracking or tearing at a macro level, FRP damage and characteristics of interest include blistering, delamination and potential creep of the resin. While certain aspects of this type of inspection are performed with respect to the condition of the steel, many of the FRP inspection methods are comparable to other well-established methods. Additional information may be found in NCHRP report 564, *Field Inspection of In-Service FRP Bridge Decks (2006)*, and Hillman's *HCB Design & Maintenance Manual* (Hillman, 2012).

### *Visual Inspection*

As noted earlier, visual inspection is a basic, cost-efficient method of initial investigation into the condition of a bridge. In the case of HCB, the focus of visual inspection is the quality of the FRP encasement. Surface defects of interest include; cracks, voids, blistering, discoloration, and delamination. Degradation of the FRP shell is an indicator of potential problem spots within, and thus further NDE testing should be performed at these locations to determine overall

HCB health. Individual beams should be rated following as closely and objectively as possible using the rating system from 0-9 provided by Hillman (2012).

### *Mechanical Sounding*

Similar to the impact echo inspection process, a mechanical sounding method such as an instrumented hammer tap test or Schmidt hammer test applies a localized impact to the surface. Rather than measuring the interaction of the stress wave throughout the material, these methods simply measure the overall energy transfer between the material and the device through mechanisms such as rebound or acoustic emission. The purpose of this type of FRP evaluation is two-fold. Most importantly, the presence of moisture adsorbed within any FRP micro-cracks would alter the acoustic impedance of the FRP at that location. Any such change in response due to the presence of water would indicate a threat to the embedded steel at that location. Furthermore, the acoustic impedance of the FRP would be altered with the delamination of the glass fiber sheets. Although delaminations are less critical than the presence of micro-cracks that open vertically and allow access to the steel, if a delaminated area were to intersect a micro-crack, the delamination could serve as a collection space for moisture within the FRP.

### *Thermography*

Thermography, as previously highlighted, is adept at locating concrete voids and delamination because of the different thermal properties exhibited by concrete, air, and water. In the case of voids or delamination, a layer of air will act as an insulator, preventing thermal conduction of energy from one mass of concrete to another. If the insulated section of concrete happens to be at or near the surface, the emissivity of this section of concrete manifest as a loss of heat greater than that of an intact section of concrete. In the presence of a moisture-saturated void, this loss of heat would be less distinct.

This theory is also applicable to the FRP used in construction of these HCBs, as several layers of glass FRP sheets are overlaid in various orientations and then vacuum-infused with a resin that binds the system monolithically. If, however, a separation between the two layers of FRP were to emerge, then thermography would be appropriate for detecting this separation, just as in concrete delamination.

### **Inspection of HCB Interior for Moisture Content**

Also of interest is the presence of moisture within the FRP shell. While the steel is embedded in the FRP, moisture that is able to penetrate the shell and foam will likely settle to the bottom of the beam, only separated from the steel with a single layer of FRP. The arch concrete would also be directly exposed to any contaminants.

### *Ground Penetrating Radar (GPR)*

The low frequency electromagnetic waves emitted from a GPR unit embody differing wave speeds depending on the material dielectric properties. This theory can be used to an advantage when investigating the moisture content of the internal foam. The presence of water

within the interior of the beam would no doubt alter the dielectric properties of the foam, and would therefore produce differing wave speeds. These waves would reflect off the back FRP and return to the transducer at specific time stamps. One would be able to scan vertically along the HCB web and identify any gradients in dielectric constant, as any water within would tend to settle towards the bottom of the beam. Such a dielectric constant gradient would indicate that there is likely moisture present. Inspectors should keep in mind the composition of the beam interior and note the location of the concrete arch and fin, where the wave would travel a shorter distance before returning to the transducer.

### *Thermography*

Thermography, which has been previously discussed, also has applications for inside the HCB. Having very high specific heat, water should show up quite readily in a thermographic scan. If moisture were to penetrate the FRP shell and infiltrate the internal foam, the water would alter the thermal properties of the foam, and a vertical thermal scan should indicate a thermal gradient as the water settles to the bottom of the beam.

## **SUMMARY OF FINDINGS**

- *Flexural load distribution behavior determined from the externally mounted strain gauges was consistent with expected trends.* The highest strains were registered directly under the load vehicle and dissipated further away for the point of load application. The parapet walls offered a significant stiffening contribution to the fascia girders. The controlling experimental distribution factors confirmed Ahsan's (2012) laboratory work, and similarly yielded distribution factors comparable to those derived for design of typical beam type bridges. For the interior girders, the controlling distribution factor exceeded the AASHTO distribution factor for the Type B (closed steel or concrete box with a concrete deck) category by ~15%, but all other measured distribution factors were lower than the design estimates.
- *The typical dynamic load allowance registered was comparable to the AASHTO design values typical for conventional bridge systems, but for some cases the HCB system exceeded this design value.* Several instances of larger amplifications (44-46%) were observed for Load Case B, which positioned the loading vehicle over the second and third most northern girders, indicating that the system may be more compliant than a traditional beam bridge, but additional evaluation may be necessary.
- *The FRP shell does not act compositely with the internal HCB components (concrete arch and prestressed strand tie).* The internal strain profiles confirm the assumed neutral axis, but showed a non-linear trend. It was shown that the arch does not act compositely with the system and the assumption that plane sections remain plane is not valid for HCB. In fact, the arch may exhibit local flexural bending within the girder that is especially apparent at the quarter-spans, but subdued at mid-span due to an additional FRP shell layer beneath the arch that provides additional stiffness.

- *There was also an observed disparity between the bottom flange strains and the strains in the tension steel. This phenomenon could be explained by slippage of the steel within the FRP flange, though this occurrence has not been experimentally verified. Another way to look at this phenomenon is debonding of the top layer of FRP due to the vertical force applied by the steel during flexure. If the steel were to separate from the outer layers of FRP, there exists insufficient vertical restraint to enforce curvature in the steel during bending, and thus the steel would experience the pure tensile strain associated with a tied arch. The FRP shell would experience the curvature of the deck through the rigidity of the FRP webs and also higher strains than the steel.*
- *The shear response of the system was not captured from the experimental program and could not be evaluated based on the research results.*

## **CONCLUSIONS**

- *The lateral load distribution can be accommodated by existing provisions of the AASHTO LRFD Bridge Design Specifications if the bridge is described as a beam (Case A) or box (Case B) type structure per AASHTO LRFD Bridge Design Specification – Table 4.6.2.2.1-1 (AASHTO, 2012).*
- *The dynamic load allowance or dynamic amplification observed from the live-load testing program was inconsistent when compared against the AASHTO LRFD Bridge Design Specifications (AASHTO, 2012).*
- *The element level load sharing response observed from the live-load testing program demonstrated that composite action exists between the HCB and the reinforced concrete deck, but a potential loss of composite action may be present within the HCB element.*

## **RECOMMENDATIONS**

1. *The Virginia Transportation Research Council (VTRC) and VDOT's Fredericksburg District should perform additional load tests of the Tides Mill Stream Bridge after 2 years of service, and potentially periodically thereafter, to determine if the bridge behavior has changed over time. After allowing for time-dependent material behavior to level out, this additional testing could be used as an indicator of changes in condition as well as changes in local component and global system behavior.*
2. *VTRC should evaluate the performance of suitable NDE methods in conjunction with the follow-up load-testing program. Currently, bridge safety inspectors can employ classical methods such as visual assessment and sounding to perform a preliminary evaluation. Determining other applicable NDE methods can better assist the inspectors in assessing the condition of the Tides Mill Stream Bridge and future structures designed with FRP materials.*

A number of potential NDE tools are currently available within VDOT/VTRC and through collaborations with local universities.

## **BENEFITS AND IMPLEMENTATION**

### **Benefits**

This project was based on a newly developed system and represented the first in-service application of HCB by VDOT. The results of the installation and current performance suggest that this solution is a viable alternative for short and medium span bridges. While this study did not consider the economics of the HCB system, there were a number of potential benefits observed that may warrant further consideration of this system. Two of these benefits are as follows:

1. The system is lightweight and allows for the re-use of existing substructure components of the bridge being replaced. While the reduction in weight was not fully realized in this particular project, the modular nature of this system could have allowed for an alternative construction method, whereby the empty FRP shells could be installed using small cranes and then filled with SCC on-site rather than in the precast plant. Hauling companies could transport multiple empty shells to the job site, thus dramatically reducing the shipping costs.
2. The modular nature of the HCB system appears to lend itself to accelerated bridge construction practices as the system could be completely prefabricated, with or without the concrete deck.

### **Implementation**

The two study recommendations will be implemented as follows:

1. *VTRC will coordinate with VDOT's Fredericksburg District and university partners in conducting a follow-up load test.* The test called for in Recommendation 1 will be conducted by the end of 2017. The additional information gathered from this load test will be shared with the Fredericksburg District and VDOT's Structure and Bridge Division.
2. *VTRC has initiated a durability study on components of the HCB.* The durability study will address Recommendation 2 through accelerated laboratory and field exposure tests in industrial and marine environments. As a part of evaluating the exposure samples, the researchers are investigating supplemental NDE methods that may also be deployed for inspecting in-service structures. That study is scheduled to be completed at the end of June 2018.

## ACKNOWLEDGMENTS

The research team thanks Andy Zickler from VDOT's Central Office, who assisted with the selection of instrumentation locations; Leslie Danovich and her inspection team from VDOT's Fredericksburg District, who provided the boats needed to install the instrumentation; VDOT's Fredericksburg District for providing the load trucks and traffic control; and Coastal Precast for allowing the researchers to observe the concrete fabrication portion of the HCBs. The project also included contributions during the field testing from Bernie Kassner from VTRC and from the following University of Virginia student researchers: Mark Saliba, Amir Gheitasi, Marc Hansen, Jonathan Tanks, and Evelina Khakimova.

## REFERENCES

- Ahsan, S. (2012). *Evaluation of Hybrid-Composite Beam for Use in Tide Mill Bridge*. Masters of Science, Virginia Tech, Blacksburg.
- American Association of State Highway and Transportation Officials. (2002). *Standard Specification for Highway Bridges*. Washington, DC.
- American Association of State Highway and Transportation Officials. (2012). *AASHTO LRFD Bridge Design Specifications, 6th ed., with 2013 Interim Revisions*. Washington, DC.
- ASTM Committee A-6. (1964). *Magnetic Testing - Theory and Nomenclature*. ASTM Special Technical Publication No. 371. ASTM International, West Conshohocken, PA.
- ASTM International. (2007). *STM D4788-03 (2007): Standard Test Method for Detecting Delaminations in Bridge Decks Using Infrared Thermography*. In *ASTM Book of Standards*. West Conshohocken, PA.
- ASTM International. (2009). *ASTM E570-09: Standard Practice for Flux Leakage Examination of Ferromagnetic Steel Tubular Products*. In *ASTM Book of Standards*. West Conshohocken, PA.
- ASTM International. (2010). *ASTM C1383 - 04(2010): Standard Test Method for Measuring the P-Wave Speed and the Thickness of Concrete Plates Using the Impact-Echo Method*. In *ASTM Book of Standards*. West Conshohocken, PA.
- Civitillo, J. (2014). *In-Service Performance and Behavior Characterization of the Hybrid-Composite Bridge System*. MS Thesis, University of Virginia, Charlottesville.
- Eom, J., and Nowak A. (2001). *Live Load Distribution for Steel Girder Bridges*. *Journal of Bridge Engineering*, Vol. 6, pp. 489-497.
- Geophysical Survey Systems Inc. (2006). *GSSI Handbook for RADAR Inspection of Concrete. I*. Geophysical Systems, Salem, NH.

- Harris, D.K. (2010). Assessment of Flexural Lateral Load Distribution Methodologies for Stringer Bridges. *Engineering Structures*, Vol. 32, No. 11, pp. 3443-3451.
- Harris, D.K., Cousins, T., Murray, T.M., and Sotelino, E.D. (2008). Field Investigation of a Sandwich Plate System Bridge Deck. *ASCE Journal of Performance of Constructed Facilities*, Vol. 22, No. 5, pp. 1-11.
- Hillman, J.R. (2003). *Investigation of a Hybrid-Composite Beam System*. IDEA Program Final Report HSR-23. Transportation Research Board, Washington, DC.
- Hillman, J.R. (2008). *Product Application of a Hybrid-Composite Beam System*. IDEA Program Final Report HSR-43. Transportation Research Board, Washington, DC.
- Hillman, J.R. (2012). Hybrid-Composite Beam (HCB®) Design & Maintenance Manual: Bridge No. BO439-MO 76 Over Beaver Creek. <http://aii.transportation.org/Documents/BMDO/HCB-design-maint-manual.pdf>. Accessed September 29, 2017.
- Hillman, J.R., and Otter, D. (2008). Testing of a Prototype Hybrid-Composite Beam Span Under Railroad Loadings. In *Proceedings of the AREMA 2008 Annual Conference*, American Railway Engineering and Maintenance-of-Way Association, Lanham, MD.
- International Atomic Energy Agency. (2002). *Guidebook on Non-Destructive Testing of Concrete Structure*. Vienna, Austria.
- International Organization for Standardization. (2012). *Eddy Current Testing—General Principles*. ISO 15549:2008. Geneva, Switzerland.
- Otter, D., and Doe, B. (2009). *Testing of a Prototype Hybrid-Composite Beam Span at FAST*. Technology Digest TD-09-019. Transportation Technology Center Inc., Pueblo, CO.
- Otter, D., and Tunna, L. (2011). *Secondary Generation Hybrid Composite Beam Span: Preliminary Assessment at Facility of Accelerated Service Testing*. Technology Digest TD-11-038. Transportation Technology Center Inc., Pueblo, CO.
- Sansalone, M. (1997). Impact-echo: The Complete Story. *ACI Structural Journal*, Vol. 94, No. 6.
- Snape, T. and Lindyberg, R. (2009). *Test Results: HC Beam for the Knickerbocker Bridge*. AEWRC Report 10-16, Project 671. University of Maine, Orono.
- Telang, N.M., Dumlao, C., Mehrabi, A.B., Ciolko, A.T., and Gutierrez, J. (2006). *Field Inspection of In-service FRP Bridge Decks*. NCHRP Report 564. Transportation Research Board, Washington, DC.

- Van Nosedall, S., Moen, C.D. , Cousins, T.E., and Roberts-Wollmann, C.L. (2013). Experiments on a Hybrid-Composite Beam for Bridge Applications. *Transportation Research Record: Journal of the Transportation Research Board*, No. 2332, pp. 43-52.
- Waldron, C.J., Cousins, T.E., Nassar, A.J., and Gomez, J.P. (2005). Demonstration of Use of High-Performance Lightweight Concrete in Bridge Superstructure in Virginia. *Journal of Performance of Constructed Facilities*, Vol. 19, No. 2, pp. 146-154.
- Washer, G., Fenwick, R., Nelson, S., and Rumbayan, R. (2013). Guidelines for Thermographic Inspection of Concrete Bridge Components in Shaded Conditions. *Transportation Research Record: Journal of the Transportation Research Board*, No. 2360, pp. 13-20.